═══REVIEW COMMONS MANUSCRIPT═══

IMPORTANT:

- Manuscripts submitted to Review Commons are peer reviewed in a journal-agnostic way.
- Upon transfer of the peer reviewed preprint to a journal, the referee reports will be available in full to the handling editor.
- The identity of the referees will NOT be communicated to the authors unless the reviewers choose to sign their report.
- The identity of the referee will be confidentially disclosed to any affiliate journals to which the manuscript is transferred.

GUIDELINES:

- For reviewers: https://www.reviewcommons.org/reviewers
- For authors: https://www.reviewcommons.org/authors

CONTACT:

The Review Commons office can be contacted directly at: office@reviewcommons.org

Title: Ubiquilin-2 liquid droplets catalyze α-synuclein fibril formation

Authors: Tomoki Takei[1,2], Yukiko Sasazawa[1,2,3], Daisuke Noshiro[4], Mitsuhiro Kitagawa[1,2], Tetsushi Kataura[2,5], Hiroko Hirawake-Mogi[1], Emi Kawauchi[2], Yuya Nakano[2], Etsu Tashiro[2]†, Tsuyoshi Saitoh[6]‡, Shigeru Nishiyama[6], Seiichiro Ogawa[2], Soichiro Kakuta[7], Saiko Kazuno[7], Yoshiki Miura[7], Viktor I Korolchuk[8], Nobuo N. Noda[4], Shinji Saiki[1,5,9], Masaya Imoto[1,2,9]*, Nobutaka Hattori[1,3,9,10]*

Affiliations

[1]Department of Neurology, Juntendo University Faculty of Medicine; Tokyo, Japan.
[2]Department of Biosciences and Informatics, Keio University; Kanagawa, Japan.
[3]Research Institute for Diseases of Old Age, Juntendo University Graduate School of Medicine; Tokyo, Japan.
[4]Institute for Genetic Medicine, Hokkaido University; Sapporo, Japan.
[5]Department of Neurology, Institute of Medicine, University of Tsukuba; Ibaraki, Japan.
[6]Department of Chemistry, Keio University; Kanagawa, Japan.
[7]Biomedical Research Core Facilities, Juntendo University Graduate School of Medicine; Tokyo, Japan.
[8]Biosciences Institute, Faculty of Medical Sciences, Campus for Ageing and Vitality, Newcastle University; Newcastle upon Tyne, UK.
[9]Division for Development of Autophagy Modulating Drugs, Juntendo University Faculty of Medicine; Tokyo, Japan
[10]Neurodegenerative Disorders Collaborative Laboratory, RIKEN Center for Brain Science; Saitama, Japan.
*Corresponding author (Masya Imoto). Email: m.imoto.xz@juntendo.ac.jp *Corresponding author (Nobutaka Hattori). Email: nhattori@juntendo.ac.jp
†Present address: Laboratory of Biochemistry, Showa Pharmaceutical University; Tokyo, Japan.
‡Present address: Institute of Medicine, University of Tsukuba, Tennodai, Tsukuba; Ibaraki, Japan.

Abstract

Liquid–liquid phase separation (LLPS) and the subsequent liquid–solid transition are thought to be common aggregation mechanisms of neurodegeneration-associated proteins. α-Synuclein (α-syn), whose aggregation represents the major pathological hallmark of Parkinson's disease, is reported to undergo LLPS, which accelerates oligomer and aggregate formation *in vitro* and *in vivo*; however, the precise molecular events involved in the early stages of α-syn aggregation remain controversial. In the present study, α-syn aggregation was promoted by liquid droplets formed by ubiquilin-2 (UBQLN2) rather than directly by the LLPS of α-syn. During the liquid–gel/solid transition of UBQLN2 droplets, α-syn within the droplets was transformed into pathogenic fibrils both *in vitro* and within cells. The small compound SO286 inhibited both UBQLN2 self-interaction and α-syn–UBQLN2 interaction by binding to the STI1 region of UBQLN2, thereby impairing α-syn aggregation. These results indicate that UBQLN2 droplets catalyze α-syn fibril formation and suggest that small molecules that target fibrillation-catalyzing proteins may represent a promising strategy for the development of therapeutics against neurodegenerative diseases.

Significance statement

Although the fibril formation of α-synuclein is a major driver of Parkinson's disease pathology, the mechanisms of its early stages remain unclear. Here, we demonstrated *in vitro* and in cells that ubiquilin-2 (UBQLN2) droplets, formed via liquid–liquid phase separation, absorbed soluble α-synuclein and promoted the fibril formation of α-synuclein through their liquid–gel/solid transition. This result suggests a previously unrecognized role for UBQLN2 in catalyzing α-synuclein fibril formation via its own liquid–liquid phase separation. Furthermore, a small molecule targeting the STI1 region of UBQLN2 inhibited both the liquid–solid transition of UBQLN2 and the interaction between UBQLN2 and α-synuclein, thereby suppressing α-synuclein aggregation. These findings suggest a new approach for the development of therapeutic interventions for Parkinson's disease.

Introduction

Some neurodegenerative disease-associated proteins form liquid droplets *via* liquid–liquid phase separation (LLPS) (1-3). These droplets then transit from a highly labile liquid state to a hydrogel state, and eventually to a solid-like condensate, over time via self-interaction and oligomerization of the proteins within, thereby leading to the formation of amyloid fibrils (4, 5). Recently, α-synuclein (α-syn) was reported to be one such protein (6-13); however, the formation of α-syn liquid droplets *in vitro* reportedly requires extremely high protein concentrations (200 μM at physiological pH), and their liquid–solid transition requires a relatively long incubation period (up to 20 days) (6). The mechanisms underlying the LLPS and liquid−solid transitions of α-syn under physiological conditions therefore remain controversial.

Ubiquilins (UBQLNs) are shuttle proteins that are involved in protein quality control for the maintenance of homeostasis (14-17). Among the five human UBQLNs, UBQLN1, UBQLN2, and UBQLN4 share highly conserved domains (18). These three UBQLNs are multidomain proteins composed of an intrinsically disordered region, which includes two STI1 (STI1-1 and STI1-2) regions flanked by the N-terminal ubiquitin-like (UBL) domain and the C-terminal ubiquitin-associated domain (19). Only UBQLN2 also contains a proline-rich region between the STI1-2 region and the ubiquitin-associated domain; this region contributes to the self-interactions of UBQLN2 (20). Recent studies have revealed that these UBQLNs undergo LLPS into liquid droplets under physiological conditions (20-22).

Although the functions of UBQLN LLPS remain unclear, it may be that UBQLN2 undergoes LLPS into membrane-less organelles or condensates, such as stress granules, to transfer ubiquitinated proteins to proteasome or autophagy systems because UBQLN2 droplets are disassembled by interactions between UBQLN2 and ubiquitin (14, 23, 24). Furthermore, UBQLN2 LLPS may contribute to the formation of intracytoplasmic inclusion bodies in neurodegenerative disorders (25-28). However, the relationship between UBQLN2 LLPS and the development of neurodegenerative diseases, such as Parkinson's disease, remains unclear. In the present study, we established the role of UBQLN2 LLPS in α-syn aggregation under physiological conditions and proposed a strategy for suppressing α-syn aggregation by using a UBQLN2-binding compound.

Results

α-Syn is incorporated into UBQLN2 liquid droplets and transformed into aggregates in vitro

UBQLN2 has been widely implicated in several neurodegenerative diseases (21, 25, 29-33), including Parkinson's disease (23, 34). We therefore examined the possible involvement of UBQLN2 LLPS in α-syn aggregation. Recombinant UBQLN2 at 10 μM (1% DyLight488-labeling) immediately underwent LLPS to form liquid droplets in the presence of 3% polyethylene glycol (PEG), which is often used to mimic an intracellular crowding environment *in vitro* (Fig. 1A). Conversely, recombinant α-syn at 10 μM (1% DyLight633-labeling) did not undergo LLPS in the presence of 3% PEG for up to 20 days. When α-syn was mixed with UBQLN2 in the presence of 3% PEG, α-syn was immediately incorporated into UBQLN2 droplets (Fig. 1A). Although a deletion mutant lacking the UBL domain of UBQLN2 formed liquid droplets within 1 h, these droplets failed to incorporate α-syn even after 120 h (Supplementary Fig. S1A).

Intriguingly, smaller-sized UBQLN2 droplets with incorporated α-syn (UBQLN2/α-syn droplets) gradually disappeared alongside the appearance of larger-sized droplets, which then began to lose their spherical shape (Fig. 1A). The transition over time of liquid droplets into more stable states is known as the liquid−gel/solid transition (35, 36). To explore whether the loss of spherical shape is caused by the liquid−gel/solid transition of UBQLN2/α-syn

droplets, we used 10% 1,6-hexanediol (1,6-HD), which is a hydrophobic reagent that inhibits liquid droplet formation (37). At 24 h, UBQLN2/α-syn droplets dissolved following the addition of 1,6-HD. By contrast, after 96 h, these droplets were resistant to 1,6-HD, suggesting that the UBQLN2/α-syn droplets had transited from a liquid to a gel/solid state (Supplementary Fig. S1B). Furthermore, although α-syn was also incorporated into UBQLN1 and UBQLN4 droplets (Fig. 1A), these droplets maintained their spherical shape for up to 96 h (Fig. 1A). UBQLN1/α-syn droplets were dissolved in 1,6-HD at both 24 and 96 h, whereas UBQLN4/α-syn droplets were resistant to 1,6-HD at both 24 and 96 h (Supplementary Fig. S1B).

α-Syn aggregation is synchronized with the liquid−gel/solid transition of UBQLN2 droplets

Fluorescence recovery after photobleaching (FRAP), which characterizes the fluidity of proteins, revealed that the fluorescence recovery rate of UBQLN2 in the droplets was much lower at 96 h than at 24 h (Fig. 1B, Supplementary Fig. S1C). Similarly, the fluorescence recovery rate of α-syn inside UBQLN2 droplets was much lower at 96 h than at 24 h (Fig. 1B, Supplementary Fig. S1C). These data suggest that α-syn dynamics decrease alongside the solidification of UBQLN2 liquid droplets. The fluorescence recovery rate of UBQLN1 was slightly greater than that of UBQLN2 at 24 h, and this fast recovery rate was maintained even at 96 h (Fig. 1C, Supplementary Fig. S1C). By contrast, the fluorescence recovery rate of UBQLN4 was significantly lower than that of UBQLN2 at both 24 and 96 h (Fig. 1B, Supplementary Fig. S1C). These results are consistent with previous findings indicating that, among the three UBQLNs, UBQLN1 is the most liquid-like and UBQLN4 is the most aggregation-prone (21). Although the fluorescence recovery rate of α-syn was similar among UBQLN1, UBQLN2, and UBQLN4 droplets at 24 h, it was much lower in the UBQLN2 droplets only at 96 h (Fig. 1B Supplementary Fig. S1C), suggesting that α-syn undergoes aggregation and solidification within UBQLN2 droplets over time.

Fibrillar species reportedly emerge from condensates upon aberrant amyloidogenic solidification (3, 6, 37); we similarly revealed that fibrillar-like species of α-syn and UBQLN2 emerged from subsets of gel/solid-state UBQLN2/α-syn droplets after 96 h of LLPS induction (Fig. 1C). Fibrillar α-syn was also detected using transmission electron microscopy. After 48 h of LLPS induction, small amyloid-like fibrils emerged from the subsets of UBQLN2/α-syn droplets and transformed into larger filaments by 72 and 96 h (Fig. 1D). Immunoelectron microscopy revealed that the amyloid-like fibrils that had formed at 96 h were positive for α-syn (Fig. 1D). Taken together, these results suggest that α-syn undergoes aggregation (the formation of oligomers and fibrils) specifically inside UBQLN2 droplets, and indicate that the liquid−gel/solid transition of droplets occurs at concentrations similar to those estimated *in vivo* (10, 20).

α-Syn directly interacts with UBQLN2

Given that α-syn was incorporated into the UBQLN2 droplets *in vitro*, we next examined whether α-syn can directly interact with UBQLN2. Recombinant α-syn-FLAG and hemagglutinin (HA)-UBQLN2 were incubated, and HA-UBQLN2 bound to α-syn-FLAG was pulled down using anti-FLAG beads and detected by western blotting using an anti-UBQLN2 antibody. Consistent with a previous finding indicating that UBQLN2 interacts with α-syn *in vivo* (38), we confirmed that α-syn directly binds to UBQLN2 *in vitro* (Fig. 2A).

To determine the region of UBQLN2 that is required for α-syn binding, the binding abilities of a series of UBQLN2 mutants with successive N- or C-terminal deletions to α-syn were evaluated using far-western blotting. UBQLN2 mutants lacking the STI1-2 region failed to bind to α-syn (Supplementary Fig. S2A), and, UBQLN2 mutants with both the UBL domain and STI1-1 bound α-syn, while those with only the UBL domain did not (Supplementary Fig. S2B). These results indicate that α-syn binds to the STI1 regions of UBQLN2. Furthermore, UBQLN2 mutantslacking the STI1-2 showed a greater decrease in α-syn binding than those lacking the STI1-1 (Fig. 2B), indicating that STI1-2 is the primary binding site for α-syn.

We next studied the interaction between UBQLN2 and α-syn via high-speed atomic force microscopy (HS-AFM), which can visualize intrinsically disordered proteins and even liquid droplets with much higher resolution than fluorescence microscopy (39, 40). Unexpectedly, HS-AFM imaging of the α-syn–UBQLN2 mixture at 1 μM revealed a complex maze of higher-order condensates covering approximately half of the mica surface (Fig. 2C). These condensates appeared to follow a pattern of spinodal decomposition—a type of LLPS caused by concentration fluctuations rather than nucleation—which might be promoted by an increase in the local protein concentration on the negatively charged mica; the physiological relevance of this change is discussed in the *Discussion*. This pattern was not observed for either UBQLN2 or α-syn alone, indicating that it is formed via direct UBQLN2–α-syn interaction (Fig. 2C).

α-Syn aggregation is facilitated by UBQLN2 droplets in cell culture

We next examined whether the UBQLN2 LLPS-mediated α-syn aggregation observed *in vitro* also occurs in cultured cells. UBQLN2 is reported to undergo LLPS and form droplets when cells are treated with stressors such as arsenite (i.e., $AsNaO_2$ oxidative stress) (20). We indeed observed that UBQLN2 formed small droplets at 3 h following $AsNaO_2$ (50 μM) treatment in SH-SY5Y cells stably expressing wild-type (WT) α-syn-enhanced green fluorescent protein (EGFP) (α-syn(WT)-EGFP/SH-SY5Y cells); over time, these droplets grew in size (Fig. 3A). In synchrony with the formation of UBQLN2 droplets, α-syn-EGFP condensates appeared 3 h after $AsNaO_2$ treatment and were almost entirely co-localized with UBQLN2 droplets (Fig. 3A), indicating that α-syn is also incorporated into UBQLN2 droplets in cultured cells. The UBQLN2/α-syn droplets grew larger over time and became

thioflavin S (ThS)-positive (Fig. 3B), indicating that protein aggregation progresses inside UBQLN2 droplets. FRAP studies also revealed a fast fluorescence recovery rate of α-syn-EGFP puncta at 3 and 6 h, but not 12 h, following $AsNaO_2$ treatment; this finding further indicates that α-syn aggregates inside UBQLN2 droplets over time (Fig. 3C, Supplementary Fig. S3A). Together, our findings suggest that α-syn is incorporated into UBQLN2 droplets formed in response to oxidative stress and undergoes aggregation during the liquid−gel/solid transition of UBQLN2 droplets in cultured cells.

To confirm whether UBQLN2 is indeed responsible for $AsNaO_2$-induced α-syn aggregation in cultured cells, we constructed UBQLN-knockout (KO) SH-SY5Y cells expressing pathogenic α-syn(A53T)-EGFP (Control-KO, UBQLN2-KO, and UBQLN1-KO cells) and monitored α-syn condensate formation. Larger α-syn condensates that grew over time were observed upon $AsNaO_2$ treatment in Control-KO and UBQLN1-KO cells but not in UBQLN2-KO cells (Supplementary Fig. S3B). Because we failed to establish UBQLN4-KO cells, the involvement of UBQLN4 in $AsNaO_2$-induced α-syn condensation was studied via small interfering RNA (siRNA)-mediated knockdown experiments. Although $AsNaO_2$ triggered the formation of larger α-syn condensates in cells with UBQLN1 or UNQLN4 knockdown, only small α-syn condensates were observed when UBQLN2 was silenced (Fig. 3D). When α-syn(WT)-EGFP/SH-SY5Y cells were treated with puromycin, which induces the LLPS of UBQLN2 (20), the formation of larger α-syn condensates was observed over time. These puromycin-induced larger α-syn condensates were observed in cells with UBQLN1 or UBQLN4 knockdown, but not in cells with UBQLN2 knockdown (Supplementary Fig. S3C). These results indicate that UBQLN2, but not UBQLN1 or UBQLN4, is responsible for the formation of large α-syn condensates in cultured cells in response to various cellular stresses.

In familial and sporadic Parkinson's disease, α-syn is extensively phosphorylated at Ser129 in synucleinopathic lesions; *in vitro*, this phosphorylation promotes α-syn fibril formation, which is a hallmark of aggregated α-syn (41, 42). Moreover, α-syn aggregates reportedly exhibit sarkosyl insolubility (43, 44). We therefore examined α-syn phosphorylation levels in the sarkosyl-insoluble fraction prepared from each UBQLN-KO or -knockdown cell line 12 h after $AsNaO_2$ treatment. The amount of Ser129-phosphorylated α-syn in the sarkosyl-insoluble fraction was increased by $AsNaO_2$ treatment in the control-KO, UBQLN1-KO, and UBQLN4-knockdown cells but not in the UBQLN2-KO cells (Fig. 3E). Collectively, these results suggest that UBQLN2 is indispensable for oxidative stress-induced α-syn aggregation in a cultured cell system.

Liquid−gel/solid transition of UBQLN2 droplets is inhibited by the UBQLN2-binding compound SO286

The compound 1,2,3,6-tetra-O-benzoyl-*muco*-inositol (SO286) (45) (Fig. 4A) was originally identified in a neuroprotective compound screening from our in-house chemical library; it

was revealed to bind to UBQLNs via a pulldown assay involving biotinylated SO286. In the present study, surface plasmon resonance analysis revealed that SO286 selectively bound to UBQLN2 with an affinity (K_d) of 0.351 μM (Fig. 4B, Supplementary Fig. S4A). An interaction analysis between biotin–SO286 and UBQLN2 truncation mutants using surface plasmon resonance identified STI1-1 and STI1-2 as the binding sites for SO286 (Fig. 4C). The deletion of either STI1-1 or STI1-2 did not reduce the affinity of UBQLN2 for SO286, indicating that these regions are redundantly involved in SO286 binding (Fig. 4D). We then investigated whether the binding of SO286 to UBQLN2 affects the formation of liquid droplets of UBQLN2 compared with UBQLN1 and UNQLN4. Each recombinant UBQLN protein (10 μM) was incubated with SO286 in the presence of PEG. After 24 h, the numbers and sizes of the UBQLN liquid droplets were not affected by SO286 treatment at concentrations up to 20 μM, indicating that SO286 did not affect the LLPS of UBQLN1, UBQLN2, or UBQLN4 (Supplementary Fig. S4B).

Next, we examined the effects of SO286 on the liquid−gel/solid transition of UBQLN2. The spherical collapse of UBQLN2 droplets over time was suppressed by treatment with SO286 in a dose-dependent manner (Fig. 4E). Furthermore, FRAP experiments revealed that the time-dependent reduction in the fluorescence recovery rate of UBQLN2 droplets was inhibited by 20 μM SO286 treatment (Fig. 4F, Supplementary Fig. S4C). These data suggest that SO286 inhibits the liquid−gel/solid transition of UBQLN2 droplets.

Because SO286 binds to STI1 regions that mediate the liquid−gel/solid transition of UBQLN2 droplets by promoting self-interaction and oligomerization (20), we speculated that SO286 might inhibit the liquid−gel/solid transition of UBQLN2 droplets by competitively inhibiting the STI1-mediated self-interaction of UBQLN2. We therefore examined the effects of SO286 on the interaction between immunoprecipitated FLAG-UBQLN2 and recombinant HA-UBQLN2; this interaction was inhibited by SO286 in a dose-dependent manner (Fig. 4G). Together, these findings suggest that SO286 inhibits the liquid−gel/solid transition of UBQLN2 droplets by inhibiting the STI1-mediated self-interaction of UBQLN2.

LLPS of the α-syn–UBQLN2 mixture via spinodal decomposition is specifically inhibited by SO286

In addition to the inhibitory effects of SO286 on UBQLN2 self-interaction, SO286 also inhibited the α-syn–UBQLN2 interaction in a dose-dependent manner (Fig. 5A). We therefore investigated the effects of SO286 on the formation of UBQLN2/α-syn droplets. When SO286 was added to UBQLN2/α-syn droplets at concentrations of up to 20 μM, no changes in the formation of UBQLN2/α-syn droplets were detected after 1 h using fluorescence microscopy (Fig. 5B, Supplementary Fig. S5A). Intriguingly, SO286 treatment specifically inhibited the spinodal decomposition of the UBQLN2/α-syn mixture but not that formed by α-syn and UBQLN1 or UBQLN4 (Fig. 5C, Supplementary Fig. S5B). These data suggest that the α-syn–UBQLN2 interaction is crucial for LLPS via the spinodal

decomposition mechanism and indicate that SO286 inhibits this mode of LLPS, presumably by inhibiting the α-syn–UBQLN2 interaction.

UBQLN2-mediated α-syn aggregation is inhibited by SO286

Because SO286 inhibited UBQLN2–UBQLN2 and UBQLN2–α-syn interactions as well as the time-dependent solidification of UBQLN2 liquid droplets (Figs. 4E–G, 5A), we examined whether SO286 inhibits the aggregation of α-syn inside UBQLN2 liquid droplets. As shown in Fig. 5B, SO286 (20 μM) did not inhibit the incorporation of α-syn into UBQLN2 liquid droplets; however, it suppressed the time-dependent spherical collapse of α-syn-incorporated UBQLN2 droplets. Moreover, FRAP analysis revealed that SO286 (20 μM) suppressed the decrease in the fluorescence recovery rate at 96 h of both α-syn and UBQLN2 in UBQLN2/α-syn droplets (Fig. 5D, Supplementary Fig. S5C). Furthermore, UBQLN2/α-syn fibrillar species emerging from the droplets were not observed upon SO286 treatment for up to 96 h (Fig. 5E). Together, these results suggest that SO286 suppresses α-syn aggregation inside UBQLN2 droplets.

Next, we examined whether SO286 can inhibit the UBQLN2 LLPS-mediated α-syn aggregation observed in cultured cells. SO286 inhibited neither $AsNaO_2$-induced UBQLN2 droplet formation nor α-syn incorporation into UBQLN2 droplets; however, it suppressed the time-dependent growth of UBQLN2/α-syn droplets in $AsNaO_2$-treated α-syn(WT)-EGFP/SH-SY5Y cells (Fig. 5F, Supplementary Fig. S5D). Moreover, ThS staining revealed that SO286 inhibited protein aggregation within UBQLN2 droplets (Fig. 5G). SO286 also reduced the amount of α-syn and Ser129-phosphorylated α-syn in sarkosyl-insoluble fractions prepared from $AsNaO_2$-treated α-syn(WT)-EGFP/SH-SY5Y cells at 12 h (Fig. 5H), and similar results were obtained when α-syn(A53T)-EGFP was expressed in SH-SY5Y cells (Supplementary Fig. S5E). Collectively, our findings indicate that SO286 inhibits α-syn aggregation by inhibiting both the α-syn–UBQLN2 interaction and the liquid−solid transition of UBQLN2 droplets.

Discussion

To date, neurodegenerative disease-associated proteins, including α-syn, are believed to form fibers on their own via their ability to undergo LLPS and the subsequent liquid−gel/solid transition (6, 7, 9-13, 46). The present findings indicate that UBQLN2 LLPS catalyzes the fibril formation of α-syn under physiological conditions that do not cause LLPS and self-fibrillation of α-syn alone. This role of UBQLN2 is conceptually distinct from its previously reported cytoprotective functions involving the proteasome or autophagy systems for the degradation of ubiquitinated proteins (14-17, 38, 47).

Our findings indicate that the early step in UBQLN2 LLPS-catalyzed α-syn fibril formation is the incorporation of α-syn into UBQLN2 droplets, followed by the interaction between UBQLN2 and incorporated α-syn. Furthermore, our results suggest that although the UBL

domain of UBQLN2 is not required for its interaction with α-syn, it is indispensable for initiating α-syn incorporation (Supplementary Figs. S1A, S2A). For the interaction between α-syn and UBQLN2, the two STI1 regions of UBQLN2—particularly the STI1-2 region—serve as binding sites for α-syn. These STI1 regions of UBQLN2 also reportedly bind to other components, such as heat shock protein 70, that are crucial for the protein quality control function of UBQLN2 (24, 48, 49). Nevertheless, the detailed binding mechanism between UBQLN2 and α-syn remains to be elucidated in future studies.

The self-association of α-syn through the hydrophobic face of the NAC domain, which is autoinhibited by the interaction between the N- and C-terminal domains, is important for LLPS and the subsequent liquid−gel/solid transition at high concentrations of α-syn alone *in vitro* (7). The binding of α-syn to UBQLN2 might change the autoinhibitory conformation of α-syn within the UBQLN2 droplets, thereby promoting NAC domain-mediated self-association and the liquid−gel/solid transition into fibrils. Notably, the observation of α-syn–UBQLN2 LLPS via the spinodal decomposition mechanism on mica at physiologically low concentrations (1 μM) might mimic the initial LLPS process of α-syn–UBQLN2 droplets in specific cellular environments, such as in negatively charged membranes that are known to affect α-syn LLPS. However, this mechanism is likely insufficient for α-syn fibrillation because UBQLN1 and UBQLN4, which undergo LLPS and interact with α-syn similarly to UBQLN2, cannot catalyze this reaction. This may be because of differences in the droplet dynamics of each UBQLN; UBQLN1 and UBQLN4 droplets are constantly liquid-like and gel/solid-like, respectively, whereas UBQLN2 droplets can undergo a liquid−gel/solid transition. The ability of UBQLN2 to both undergo the liquid−gel/solid transition and bind to α-syn may be essential for catalyzing α-syn fibrillation.

Consistent with this concept, SO286—a compound that binds to the STI1 regions of UBQLN2, which contain the binding sites of α-syn to UBQLN2—inhibited α-syn fibrillation by disrupting both UBQLN2 self-interaction (required for the liquid−gel/solid transition of droplets) and α-syn–UBQLN2 interaction. Intriguingly, although SO286 did not inhibit UBQLN2 LLPS *in vitro* or in cells, it inhibited α-syn–UBQLN2 LLPS on negatively charged mica and inhibited the formation of large UBQLN2 droplets in cells. In contrast to an *in vitro* system that contains only purified proteins and PEG, many factors likely affect UBQLN2 and α-syn LLPS in cells. We are currently conducting research to establish cells derived from Parkinson's disease patients and an animal model system, to evaluate the clinical potential of SO286.

Although further studies are required to elucidate the detailed mechanisms of α-syn fibrillation *in vivo*, our findings provide a concept of the UBQLN2 LLPS-catalyzed fibrillation of α-syn and demonstrate the effects of UBQLN2 LLPS modulation by an STI1 region-targeted compound in the context of neurodegenerative disease development.

During the preparation of this manuscript, it has been reported that α-syn interacts with vesicle-associated membrane protein 2 to form droplets with synaptic vesicles (50, 51), and that β-syn delays the liquid−solid transition of α-syn (52). Both of these findings may also prevent α-syn pathological aggregation. By contrast, Ca^{2+} influx-induced RNA G-quadruplex assembly has been reported to accelerate α-syn phase transition and aggregation (53). Together with our findings, these results suggest that α-syn aggregation is regulated by phase separation with different interacting proteins and RNAs and is dependent on stress and intracellular conditions.

Materials and Methods

Materials

The SO286 was a kind gift from Professor Emeritus Seiichiro Ogawa of Keio University. Biotin–SO286 was purchased from NARD Institute, Ltd. Sodium arsenite ($AsNaO_2$) was purchased from Sigma-Aldrich. The 1,6-hexanediol was purchased from Tokyo Chemical Industry.

Cell culture

SH-SY5Y cells (ATCC #CRL-2266) and HEK293T cells (ATCC #CRL-3216) were cultured in Dulbecco's Modified Eagle Medium (MEM) supplemented with 10% fetal bovine serum, 100 U/mL penicillin/streptomycin (Nacalai Tesque), MEM nonessential amino acid solution (Thermo Fisher Scientific), 1 mM sodium pyruvate, and 2 mM L-glutamine at 37 °C with 5% CO_2. SH-SY5Y cells stably expressing α-syn(WT)-EGFP and α-syn(A53T)-EGFP were established via the transfection of the respective vectors into SH-SY5Y cells using Lipofectamine 3000 (Thermo Fisher Scientific), followed by selection with G418 (Roche Diagnostics). The KO cell lines were generated using a lentiviral expression system. Single guide RNA (sgRNA) sequences targeting the *UBQLN2* and *UBQLN1* genes were designed using the CHOPCHOP tool (54). These nontargeting sgRNA sequences for generating Control-KO cells (5′-CGCAGTCATTCGATAGGAAT-3′) (55), UBQLN2 (5′-CGCGGTGCCCGAGAACAGCT-3′), and UBQLN1 (5′-GACATTAGCAACGGAAGCCC-3′) were inserted into the BsmbI sites of a lentiCRISPRv2-blast plasmid (Addgene plasmid 83480) using standard techniques. HEK293T cells were transiently co-transfected with lentiviral vectors using PEI MAX reagent (Polysciences). Four hours after transfection, the medium was replaced with fresh culture medium. After culturing for 72 h, growth medium containing the lentivirus was collected. SH-SY5Y cells stably expressing α-syn(WT)-EGFP and α-syn(A53T)-EGFP were incubated with the collected virus-containing medium for 48 h. Uninfected cells were removed using 5 μg/mL blasticidin S (Wako). UBQLN1, UBQLN2 and UBQLN4 triple-KO T-Rex293 cells (kindly provided by Professor Eisuke Itakura, Chiba University) (56) were cultured in Dulbecco's MEM supplemented with 10% fetal bovine

serum, 100 U/mL penicillin/streptomycin, MEM nonessential amino acid mixture, 1 mM sodium pyruvate, and 2 mM L-glutamine at 37 °C with 5% CO_2.

Expression and purification of recombinant proteins

UBQLN1, UBQLN2, UBQLN4, HA-UBQLN2, and α-syn were amplified, subcloned, and inserted into the pGEX-6p-1 vector (Cytiva). Glutathione S-transferase (GST)-tagged proteins were expressed in the *Escherichia coli* strain (TaKaRa) in Luria–Bertani broth (Nacalai Tesque) at 37 °C overnight. Bacteria were induced with isopropyl β-D-1-thiogalactopyranoside and harvested after 4 h at 37 °C. The bacterial pellets were frozen, lysed in phosphate-buffered saline (PBS; TaKaRa) containing 0.1% Triton X-100 and protease inhibitor cocktail (Merck Millipore), and cleared by centrifugation at 13,000 × *g* for 15 min at 4 °C. GST-tagged proteins were purified using a Glutathione Sepharose 4 Fast Flow (Cytiva). To cleave the GST tags, the beads were incubated with PreScission Protease (Cytiva) for 16 h at 4 °C. Flow-through fractions containing unlabeled recombinant proteins were collected and concentrated, and the buffer was exchanged with LLPS buffer (200 mM NaCl, 20 mM sodium phosphate, and 0.5 mM ethylenediaminetetraacetic acid; pH 6.8) using an Amicon Ultra Centrifugal Filter (Merck Millipore).

Fluorescent labeling

UBQLN1, UBQLN2, and UBQLN4 were fluorescently labeled with DyLight488 NHS Ester (Thermo Fisher Scientific) and α-syn was fluorescently labeled with DyLight633 NHS Ester (Thermo Fisher Scientific) according to the manufacturer's instructions.

Imaging of LLPS

The UBQLN1, UBQLN2, and UBQLN4 constructs were prepared to contain 10 μM protein (spiked with DyLight488-labeled UBQLN1, UBQLN2, or UBQLN4 at a 1:100 molar ratio) in LLPS buffer containing 3% PEG (for UBQLN2 and 4) or 5% PEG (for UBQLN1). These samples were mixed with 10 μM α-syn (spiked with DyLight633-labeled α-syn, 1:100 molar ratio), and SO286 was added to a 96-well glass bottom plate (Mattek) and incubated with 3% BSA (Sigma-Aldrich) to reduce the rapid coating of the protein droplets onto the glass surface. Phase separation was imaged using a BZ-X810 fluorescence microscope (Keyence).

***In vitro* pulldown assays**

To detect the interaction between UBQLN2 and α-syn-FLAG, HEK293T cells were transfected 24 h after seeding using Lipofectamine 3000 with α-syn-FLAG. Forty-eight hours post-transfection, the cells were lysed in BA100 buffer (20 mM Tris-HCl [pH 7.5], 100 mM NaCl, 0.1% Triton-X 100, and proteinase inhibitor). The cell lysates were then incubated with anti-FLAG beads (Wako) for 3 h at 4 °C with constant rotation. The α-syn-FLAG/anti-FLAG beads were washed twice with BA100 buffer and three times with LLPS buffer before

being incubated with either UBQLN1, UBQLN2, or UBQLN4 recombinant proteins for 2 h at 4 °C with constant rotation. The beads were then washed three times with LLPS buffer and eluted with FLAG peptide (Wako). Next, the samples were loaded onto a 10%–20% Bis-tris gel and the proteins were separated via sodium dodecyl sulfate polyacrylamide gel electrophoresis (SDS-PAGE). Proteins were then transferred onto a polyvinylidene fluoride (PVDF) membrane and probed with specific antibodies, followed by detection using West Dura Extended Duration Substrate (Thermo Fisher Scientific).

To detect the self-interaction of UBQLN2, the UBQLN1, UBQLN2, and UBQLN4 triple-KO T-Rex293 cells were transfected 24 h after seeding using Lipofectamine 3000 with FLAG-UBQLN2. Forty-eight hours post-transfection, the cells were lysed in BA100 buffer. The cell lysates were then incubated with anti-FLAG beads for 3 h at 4 °C with constant rotation. Next, the FLAG-UBQLN2/anti-FLAG beads were washed twice with BA100 buffer and three times with LLPS buffer before being incubated with HA-UBQLN2 recombinant protein for 2 h at 4 °C with constant rotation. The beads were then washed three times with LLPS buffer and eluted with FLAG peptide. The samples then underwent SDS-PAGE and probing with antibodies using the same protocol as for the detection of interactions between UBQLN2 and α-syn-FLAG.

The primary antibodies were as follows: anti-UBQLN1 (Cell Signaling Technology Inc., #14526), anti-UBQLN2 (Novus Biologicals, NBP2-25164), anti-UBQLN4 (Santa Cruz, sc-136145), and anti-FLAG (Wako, 018-22381).

Far-western blotting

Far-western blotting was conducted using a method modified from Wu et al (57). Each UBQLN2-HA mutant was resolved using SDS-PAGE and transferred onto a PVDF membrane. The membrane was then blocked with blocking buffer (1% bovine serum albumin [BSA], 20 mM Tris-HCl [pH 7.5], and 1 mM dithiothreitol) containing 0.05% Tween 20 for 1 h at room temperature, incubated with 20 μM His-α-syn recombinant protein in blocking buffer overnight at 4°C, and washed with washing buffer (10 mM Tris-HCl and 100 mM NaCl). Next, the membrane was fixed with 4% paraformaldehyde (FUJIFILM Wako Pure Chemical) and 0.02% glutaraldehyde (Nacalai Tesque) at room temperature for 30 min and washed with washing buffer. The His-α-syn protein that remained bound to the UBQLN2-HA mutants on the membrane was then probed using an anti-α-syn monoclonal antibody (Abcam, ab138501) for 3 h at room temperature. Subsequently, the membrane was washed twice using washing buffer containing 0.02% Tween 20 to remove unbound antibodies. Bound antibodies were then detected using West Dura Extended Duration Substrate.

FRAP

FRAP experiments were performed using an LSM880 confocal laser scanning microscope (Carl Zeiss). Images were acquired via a 488-nm or 633-nm laser at a 100-ms exposure.

Images were taken every 1 s over 70 s. Images from each dataset were analyzed in ImageJ Fiji (version: 1.54f) (58) to measure the fluorescent intensity over time, thus generating FRAP curves for the images. The data points were fitted to a single-exponential equation to determine the recovery time.

Transmission electron microscopy

For conventional electron microscopy, samples were fixed with 2.5% glutaraldehyde (TAAB) in 0.1 M phosphate buffer (pH 7.4). Fixed samples were then dehydrated through a graded ethanol series and embedded in Epok812 (Oken Shoji). Ultrathin sections were cut before being stained with uranyl acetate and lead citrate, and were then examined using a transmission electron microscope (JEM-1400 Flash, JEOL). For immunoelectron microscopy, the samples were blocked with 1% BSA in PBS for 10 min, incubated with anti-α-syn (Abcam, ab138501) for 4 h, and then incubated with a secondary antibody (6 nm colloidal gold anti-rabbit IgG, Jackson ImmunoResearch) for 4 h at room temperature. After being washed with PBS, the samples were fixed and embedded as for conventional electron microscopy.

Immunofluorescence

Cells grown on glass coverslips were fixed and permeabilized with FP solution (2% paraformaldehyde [FUJIFILM Wako Pure Chemical], 0.25% Triton-X 100 [FUJIFILM Wako Pure Chemical]) at room temperature for 10 min before being further fixed with 2% paraformaldehyde at room temperature for 20 min. Coverslips were washed with PBS prior to blocking with 5% goat serum (Sigma-Aldrich) in 0.25% Triton X-100 for 1 h at room temperature. The cells were incubated with primary antibody for 3 h at room temperature, and then with secondary antibody for 2 h at room temperature in the dark. Primary and secondary antibodies were diluted in 3% BSA (Sigma-Aldrich) and 0.25% Triton X-100 solution. After the primary and secondary antibody incubations, three five-minute washes with PBS containing 0.25% Triton X-100 were performed at room temperature on an orbital shaker. Coverslips were mounted with Prolong Gold (Thermo Fisher Scientific) mounting media, and the immunostaining was observed and imaged using an LSM880 confocal laser scanning microscope.

ThS staining

Cells grown on glass coverslips were fixed and permeabilized with a solution containing 2% paraformaldehyde and 0.25% Triton-X 100 in PBS at room temperature for 10 min, and then further fixed with 2% paraformaldehyde at room temperature for 20 min. Coverslips were washed with PBS and incubated with 0.1% ThS (Sigma-Aldrich) in PBS, and were then immunostained with anti-UBQLN2 (Novus Biologicals, NBP2-25164) using the same

protocol as for immunofluorescence. Cells on the coverslips were observed and imaged using an LSM880 confocal laser scanning microscope.

siRNA transfection

The siRNAs targeting UBQLN1, UBQLN2, and UBQLN4 were kindly provided by the activities of the Molecular Profiling Committee, Grant-in-Aid for Scientific Research on Innovative Areas "Advanced Animal Model Support." The noncoding siRNA was purchased from Dharmacon. The SH-SY5Y cells were transfected with siRNAs using Lipofectamine RNAiMax (Thermo Fisher Scientific) in accordance with the manufacturer's instructions.

Subcellular fractionation using sarkosyl

Cells were resuspended in A68 buffer (10 mM Tris-HCl [pH 7.4], 800 mM NaCl, 1 mM ethylenediaminetetraacetic acid, 0.5 mM egtazic acid, 10% sucrose, and proteinase inhibitor) and lysed by passing the samples 10 times through a 26-G needle (TERUMO). The cell lysates were then incubated with 2% sarkosyl in A68 buffer on ice for 30 min with constant rotation before being centrifuged at 100,000 × *g* for 20 min at 4 °C. The resulting pellet and supernatant were designated the sarkosyl-soluble and -insoluble fractions, respectively. After a bicinchoninic acid assay was performed to adjust the protein concentrations, SDS-PAGE and immunoblotting analyses were performed for each fraction.

Binding analysis via surface plasmon resonance assay

A surface plasmon resonance assay was performed using a BIAcore T200 instrument (Cytiva). The sensor chip streptavidin was obtained from Cytiva. First, 1 μM biotin–SO286 was fixed onto the sensor chip according to the manufacturer's instructions. Next, UBQLN2 or HA-UBQLN2 constructs were injected at 30 μL/min over a 2-min period in PBS containing 0.05% Tween 20 (Wako) and 1 mg/mL BSA as the running buffer. The regeneration of the sensor chip was then performed using 10 mM glycine (pH 1.5) and 0.5% Tween 20 buffer. A reference flow cell (i.e., flow cell with biotin) was used for each binding analysis of biotin–SO286. Specific binding was quantified by subtracting the ligand response from the reference response. Kinetic constants were calculated using a 1:1 binding model with BIAcore T200 evaluation software ver. 2.0 (Cytiva).

HS-AFM

The HS-AFM observations were performed in tapping mode using a sample scanning HS-AFM instrument (MS-NEX, Research Institute of Biomolecule Metrology Co., Ltd.) and cantilevers (length: approximately 7 μm, width: approximately 2 μm, thickness: approximately 0.08 μm, resonant frequency: 1.2 MHz in air, and spring constant: 0.15 N/m) with electron beam-deposited tips (USC-F1.2-k0.15, NanoWorld) (59).

For the imaging of UBQLN2 and α-syn, one drop (approximately 2 μL) of UBQLN2 (1 μM) or α-syn solution (1 μM) was deposited onto freshly cleaved mica that was glued to the top of a glass stage (diameter, 1.5 mm; height, 2 mm). For the imaging of the α-syn and UBQLN2 mixture, α-syn solution (1 μM) was mixed with UBQLN2 solution (1 μM), and one drop (approximately 2 μL) of the mixture was deposited onto freshly cleaved mica. For the imaging of the α-syn and UBQLN1, UBQLN2, or UBQLN4 mixture in the presence or absence of SO286, SO286 (0.25 mM, dissolved in dimethyl sulfoxide) or dimethyl sulfoxide was premixed with UBQLN1, UBQLN2, or UBQLN4 solution (1 μM) and incubated for 5 min. The α-syn solution (1 μM) was then added, and one drop (approximately 2 μL) of the mixture was deposited onto freshly cleaved mica. For each observation, the mica was rinsed after incubation for 3 min and immersed in a liquid cell containing approximately 90 μL of imaging buffer (150 mM NaCl and 20 mM 4-[2-hydroxyethyl]-1-piperazineethanesulfonic acid-NaOH [pH 7.5]). The imaging conditions were as follows: scan size (pixel size, imaging rate), 600 × 600 nm^2 (150 × 150 pixels, 2 frames/s) or 200 × 200 nm^2 (120 × 120 pixels, 4 frames/s). Imaging was performed at 23 °C. The HS-AFM data were viewed and analyzed using Kodec4.4.7.39 software (60).

The calculation of the percentage area covered by proteins was conducted using the 'Auto Threshold' and 'Analyze Particles' functions of ImageJ software. The values were calculated from images (600 × 600 nm^2) obtained from three independent experiments.

Statistical analysis

Statistical analysis was performed using Graph Pad Prism (ver. 9.4.1) software (GraphPad Software). Details of each statistical method are shown in the respective figure legends.

Competing interests

Authors declare that they have no competing interests.

Data and materials availability

All data are available in the main text or the supplementary materials.

Acknowledgments

We thank K. Okuma for technical assistance with electron microscopy, and A. Matsumoto and K. Hoshino for assistance with target identification of SO286. We also thank Prof. Eisuke Itakura at Chiba University for kindly providing T-Rex293 cells.

We thank the Research Institute for Diseases of Old Age, the Laboratory of Proteomics and Biomolecular Science, the Laboratory of Molecular and Biochemical Research, and the Laboratory of Cell Biology, Biomedical Research Core Facilities and Juntendo University Graduate School of Medicine for technical assistance.

We thank Bronwen Gardner, PhD, from Edanz (https://jp.edanz.com/ac) for editing a draft of this manuscript.
This work was supported by JSPS KAKENHI (Grant No. 18H02099 and 21H02072 to M.I., Grant No. 24K10651 and 23K20044 to Y.S, Grant No. 21H04820 and 24H00068 to N.H. from The Ministry of Education, Culture, Sports, Science and Technology, Japan, and by JSPS KAKENHI Grant Number JP22H04922 (AdAMS) to M.I, and AMED (Grant No. 24wm0625503h0001) to N.H.

Author contributions

M.I., S.S. and N.N. designed research. T.T. performed the most of experiments. Y.S. performed chemical screening to identify SO286, and identified molecular target of SO286 with E.K., E.T., Y.N. and T.K. T.S., S.N. and S.O. synthesized biotinylated SO286. S.Kakuta performed and analysed Transmission electron microscopy studies. H.H.M. performed Far0Western blotting and H.H.M., S.Kazuno and Y.M. performed and analysed the surface plasmon resonance studies. D.N. and N.N. performed and analysed HS-AFM studies. M.K. generated and analysed several α-Syn-expressing SH-SY5Y cell lines. M.I. and N.H. acquired funding and supervised the work. T.T. and M.I. wrote the original draft. Y.S., V.I.K., N.N., S.S., M.I. and N.H. contributed to manuscript writing and editing. All of the authors discussed the results and contributed to the final manuscript. Conceptualization: M.I., S.S., N.N.N.

Refarences

1. S. Wegmann *et al.*, Tau protein liquid-liquid phase separation can initiate tau aggregation. *EMBO J* **37** (2018).
2. L. A. Gruijs da Silva *et al.*, Disease-linked TDP-43 hyperphosphorylation suppresses TDP-43 condensation and aggregation. *EMBO J* **41**, e108443 (2022).
3. A. Patel *et al.*, A Liquid-to-Solid Phase Transition of the ALS Protein FUS Accelerated by Disease Mutation. *Cell* **162**, 1066-1077 (2015).
4. S. F. Banani, H. O. Lee, A. A. Hyman, M. K. Rosen, Biomolecular condensates: organizers of cellular biochemistry. *Nat Rev Mol Cell Biol* **18**, 285-298 (2017).
5. S. Alberti, A. Gladfelter, T. Mittag, Considerations and Challenges in Studying Liquid-Liquid Phase Separation and Biomolecular Condensates. *Cell* **176**, 419-434 (2019).
6. S. Ray *et al.*, alpha-Synuclein aggregation nucleates through liquid-liquid phase separation. *Nat Chem* **12**, 705-716 (2020).
7. A. S. Sawner *et al.*, Modulating alpha-Synuclein Liquid-Liquid Phase Separation. *Biochemistry* **60**, 3676-3696 (2021).
8. B. Xu *et al.*, Manganese promotes alpha-synuclein amyloid aggregation through the induction of protein phase transition. *J Biol Chem* **298**, 101469 (2022).

9. S. Mukherjee *et al.*, Liquid-liquid Phase Separation of α-Synuclein: A New Mechanistic Insight for α-Synuclein Aggregation Associated with Parkinson's Disease Pathogenesis. *J Mol Biol* **435**, 167713 (2023).
10. L. Piroska *et al.*, α-Synuclein liquid condensates fuel fibrillar α-synuclein growth. *Sci Adv* **9**, eadg5663 (2023).
11. M. C. Hardenberg *et al.*, Observation of an α-synuclein liquid droplet state and its maturation into Lewy body-like assemblies. *J Mol Cell Biol* **13**, 282-294 (2021).
12. M. Poudyal, A. Sakunthala, S. Mukherjee, L. Gadhe, S. K. Maji, Phase separation and other forms of α-Synuclein self-assemblies. *Essays Biochem* **66**, 987-1000 (2022).
13. S. Mukherjee, M. Poudyal, K. Dave, P. Kadu, S. K. Maji, Protein misfolding and amyloid nucleation through liquid-liquid phase separation. *Chem Soc Rev* **53**, 4976-5013 (2024).
14. M. F. Kleijnen *et al.*, The hPLIC proteins may provide a link between the ubiquitination machinery and the proteasome. *Mol Cell* **6**, 409-419 (2000).
15. E. S. Stieren *et al.*, Ubiquilin-1 is a molecular chaperone for the amyloid precursor protein. *J Biol Chem* **286**, 35689-35698 (2011).
16. H. S. Ko, T. Uehara, K. Tsuruma, Y. Nomura, Ubiquilin interacts with ubiquitylated proteins and proteasome through its ubiquitin-associated and ubiquitin-like domains. *FEBS Lett* **566**, 110-114 (2004).
17. D. Y. Lee, D. Arnott, E. J. Brown, Ubiquilin4 is an adaptor protein that recruits Ubiquilin1 to the autophagy machinery. *EMBO Rep* **14**, 373-381 (2013).
18. I. Marin, The ubiquilin gene family: evolutionary patterns and functional insights. *BMC Evol Biol* **14**, 63 (2014).
19. T. Zheng, Y. Yang, C. A. Castaneda, Structure, dynamics and functions of UBQLNs: at the crossroads of protein quality control machinery. *Biochem J* **477**, 3471-3497 (2020).
20. T. P. Dao *et al.*, Ubiquitin Modulates Liquid-Liquid Phase Separation of UBQLN2 via Disruption of Multivalent Interactions. *Mol Cell* **69**, 965-978 e966 (2018).
21. J. E. Gerson *et al.*, Shared and divergent phase separation and aggregation properties of brain-expressed ubiquilins. *Sci Rep* **11**, 287 (2021).
22. T. P. Dao *et al.*, Mechanistic insights into enhancement or inhibition of phase separation by different polyubiquitin chains. *EMBO reports* **23**, e55056 (2022).
23. S. S. Sandoval-Pistorius *et al.*, Ubiquilin-2 regulates pathological alpha-synuclein. *Sci Rep* **13**, 293 (2023).
24. Q. L. Ma *et al.*, UBQLN2 and HSP70 participate in Parkin-mediated mitophagy by facilitating outer mitochondrial membrane rupture. *Embo Reports* **24** (2023).
25. N. Safren *et al.*, Pathogenic mutations in UBQLN2 exhibit diverse aggregation propensity and neurotoxicity. *Sci Rep* **14**, 6049 (2024).

26. E. J. Alexander *et al.*, Ubiquilin 2 modulates ALS/FTD-linked FUS-RNA complex dynamics and stress granule formation. *Proc Natl Acad Sci U S A* **115**, E11485-E11494 (2018).
27. L. M. Sharkey *et al.*, Mutant UBQLN2 promotes toxicity by modulating intrinsic self-assembly. *Proc Natl Acad Sci U S A* **115**, E10495-E10504 (2018).
28. T. P. Dao *et al.*, ALS-Linked Mutations Affect UBQLN2 Oligomerization and Phase Separation in a Position- and Amino Acid-Dependent Manner. *Structure* **27**, 937-951.e935 (2019).
29. H. X. Deng *et al.*, Mutations in UBQLN2 cause dominant X-linked juvenile and adult-onset ALS and ALS/dementia. *Nature* **477**, 211-215 (2011).
30. A. C. Fahed *et al.*, UBQLN2 mutation causing heterogeneous X-linked dominant neurodegeneration. *Ann Neurol* **75**, 793-798 (2014).
31. B. C. Lin, N. R. Higgins, T. H. Phung, M. J. Monteiro, UBQLN proteins in health and disease with a focus on UBQLN2 in ALS/FTD. *FEBS J* **289**, 6132-6153 (2022).
32. K. L. Williams *et al.*, UBQLN2/ubiquilin 2 mutation and pathology in familial amyotrophic lateral sclerosis. *Neurobiol Aging* **33**, 2527.e2523-2510 (2012).
33. M. Synofzik *et al.*, Screening in ALS and FTD patients reveals 3 novel UBQLN2 mutations outside the PXX domain and a pure FTD phenotype. *Neurobiol Aging* **33**, 2949.e2913-2947 (2012).
34. F. Mori *et al.*, Ubiquilin immunoreactivity in cytoplasmic and nuclear inclusions in synucleinopathies, polyglutamine diseases and intranuclear inclusion body disease. *Acta Neuropathol* **124**, 149-151 (2012).
35. D. Kaganovich, There Is an Inclusion for That: Material Properties of Protein Granules Provide a Platform for Building Diverse Cellular Functions. *Trends Biochem Sci* **42**, 765-776 (2017).
36. N. N. Noda, Z. Wang, H. Zhang, Liquid-liquid phase separation in autophagy. *J Cell Biol* **219** (2020).
37. W. M. Babinchak *et al.*, The role of liquid-liquid phase separation in aggregation of the TDP-43 low-complexity domain. *J Biol Chem* **294**, 6306-6317 (2019).
38. S. S. Sandoval-Pistorius *et al.*, Ubiquilin-2 regulates pathological alpha-synuclein. *Scientific Reports* **13**, 293 (2023).
39. A. Yamasaki *et al.*, Liquidity Is a Critical Determinant for Selective Autophagy of Protein Condensates. *Mol Cell* **77**, 1163-1175 e1169 (2020).
40. Y. Fujioka *et al.*, Phase separation organizes the site of autophagosome formation. *Nature* **578**, 301-305 (2020).
41. H. Fujiwara *et al.*, α-Synuclein is phosphorylated in synucleinopathy lesions. *Nat Cell Biol* **4**, 160-164 (2002).

42. J. P. Anderson *et al.*, Phosphorylation of Ser-129 is the dominant pathological modification of alpha-synuclein in familial and sporadic Lewy body disease. *J Biol Chem* **281**, 29739-29752 (2006).
43. L. W. Ko, H. H. Ko, W. L. Lin, J. G. Kulathingal, S. H. Yen, Aggregates assembled from overexpression of wild-type alpha-synuclein are not toxic to human neuronal cells. *J Neuropathol Exp Neurol* **67**, 1084-1096 (2008).
44. A. Ikeda *et al.*, Mutations in CHCHD2 cause α-synuclein aggregation. *Human Molecular Genetics* **28**, 3895-3911 (2019).
45. S. Ogawa, S. Oki, T. Suami, Inositol Derivatives. 11. Synthesis of Dianhydroinositols. *Bull Chem Soc Jpn* **52**, 1095-1101 (1979).
46. B. Xu *et al.*, Manganese promotes α-synuclein amyloid aggregation through the induction of protein phase transition. *J Biol Chem* **298**, 101469 (2022).
47. I. M. Valentino *et al.*, Phase separation of polyubiquitinated proteins in UBQLN2 condensates controls substrate fate. *Proc Natl Acad Sci U S A* **121**, e2405964121 (2024).
48. R. Hjerpe *et al.*, UBQLN2 Mediates Autophagy-Independent Protein Aggregate Clearance by the Proteasome. *Cell* **166**, 935-949 (2016).
49. T. Y. Zheng, S. K. K. Galagedera, C. A. Castañeda, Previously uncharacterized interactions between the folded and intrinsically disordered domains impart asymmetric effects on UBQLN2 phase separation. *Protein Sci* **30**, 1467-1481 (2021).
50. A. Agarwal *et al.*, VAMP2 regulates phase separation of α-synuclein. *Nat Cell Biol* **26**, 1296-1308 (2024).
51. C. Wang *et al.*, VAMP2 chaperones α-synuclein in synaptic vesicle co-condensates. *Nat Cell Biol* **26**, 1287-1295 (2024).
52. X. Li *et al.*, β-synuclein regulates the phase transitions and amyloid conversion of α-synuclein. *Nat Commun* **15**, 8748 (2024).
53. K. Matsuo *et al.*, RNA G-quadruplexes form scaffolds that promote neuropathological α-synuclein aggregation. *Cell* 10.1016/j.cell.2024.09.037 (2024).
54. K. Labun *et al.*, CHOPCHOP v3: expanding the CRISPR web toolbox beyond genome editing. *Nucleic Acids Res* **47**, W171-w174 (2019).
55. O. Shalem *et al.*, Genome-scale CRISPR-Cas9 knockout screening in human cells. *Science* **343**, 84-87 (2014).
56. E. Itakura *et al.*, Ubiquilins Chaperone and Triage Mitochondrial Membrane Proteins for Degradation. *Mol Cell* **63**, 21-33 (2016).
57. Y. Wu, Q. Li, X. Z. Chen, Detecting protein-protein interactions by Far western blotting. *Nat Protoc* **2**, 3278-3284 (2007).
58. C. A. Schneider, W. S. Rasband, K. W. Eliceiri, NIH Image to ImageJ: 25 years of image analysis. *Nat Methods* **9**, 671-675 (2012).

59. T. Uchihashi, N. Kodera, T. Ando, Guide to video recording of structure dynamics and dynamic processes of proteins by high-speed atomic force microscopy. *Nat Protoc* **7**, 1193-1206 (2012).
60. K. X. Ngo, N. Kodera, E. Katayama, T. Ando, T. Q. Uyeda, Cofilin-induced unidirectional cooperative conformational changes in actin filaments revealed by high-speed atomic force microscopy. *Elife* **4** (2015).

Legends for Figures

Figure 1. α-Synuclein (α-syn) aggregates within ubiquilin (UBQLN)2 droplets *in vitro*.

(*A*) Fluorescence microscopy images of individual solutions of 10 μM of each UBQLN construct (1% DyLight488-labeling) and 10 μM α-syn construct (1% DyLight633-labeling), as well as mixed solutions of each UBQLN with α-syn. (*B*) Fluorescence recovery after photobleaching (FRAP) analysis of droplets of UBQLN2 (*a*), UBQLN1 (*b*), and UBQLN4 (*c*) incorporating α-syn. Plots show the average FRAP recovery curves from 10 separate droplets. Values are the means ± standard deviations (SDs) (*Left*). Quantification of fractional recovery at 70 s after photobleaching from 10 separate droplets. *p < 0.05, **p < 0.01, ****p < 0.0001, N.S., nonsignificant (Welch's t-test). Values are the means ± SDs (*Right*). (*C*) Fluorescence microscopy images of mixed solutions of 10 μM UBQLN2 construct (1% DyLight488-labeling) and 10 μM α-syn construct (1% DyLight633-labeling) after incubation at 37 °C for 24 and 96 h. (*D*) Transmission electron microscopy images of UBQLN2 droplets incorporating α-syn at 48, 72, and 96 h after UBQLN2 liquid–liquid phase separation (LLPS) induction. Immunoelectron microscopy images of UBQLN2 droplets incorporating α-syn at 96 h after UBQLN2 LLPS induction using immuno-gold-labeled α-syn (6-nm gold particles).

Figure 2. α-Syn directly interacts with UBQLN2.

(*A*) Recombinant α-syn-FLAG and each hemagglutinin (HA)-UBQLN were incubated before α-syn-FLAG was pulled down with anti-FLAG beads and α-syn-FLAG was eluted with the FLAG peptide. The eluates were then immunoblotted with the indicated antibodies. (*B*) (*a*) Illustrations of the ΔSTI1-1/UBQLN2 mutant and the ΔSTI1-2/UBQLN2 mutant. Each UBQLN2-HA mutant was subjected to sodium dodecyl sulfate polyacrylamide gel electrophoresis (SDS-PAGE) and stained with Coomassie brilliant blue (CBB) (*b*) or transferred onto a membrane; the membrane was then incubated with recombinant His-α-syn, followed by detection using an anti-α-syn antibody (*c*).(*C*) (*a*) High-speed atomic force microscopy (HS-AFM) images of UBQLN2 covering a mica surface. UBQLN2 (1 μM) was applied to mica. (*b*) HS-AFM images of α-syn proteins. α-Syn (1 μM) was applied to mica.

(*c*) HS-AFM images of spinodal decomposition-like patterns caused by UBQLN2 and α-syn. A mixture of UBQLN2 (1 μM) and α-syn (1 μM) was applied to mica.

Figure 3. α-Syn aggregates within UBQLN2 droplets in cultured cells.
(*A* and *B*) α-Syn(WT)-EGFP/SH-SY5Y cells were stimulated with 50 μM sodium arsenite ($AsNaO_2$) for 3, 6, and 12 h and immunostained with anti-UBQLN2 and Hoechst (*A*) and with anti-UBQLN2 and ThS (*B*). Large UBQLN2 or α-syn puncta are indicated by white arrows.(*C*) FRAP analysis of α-syn condensates. α-Syn(WT)-EGFP/SH-SY5Y cells were treated with 50 μM $AsNaO_2$ for 3, 6, and 12 h. Plots display average FRAP recovery curves from 10 separate droplets. (*D*) (a) Fluorescence microscopy of α-syn(WT)-EGFP/SH-SY5Y cells with UBQLN knockdown. Cells were transfected with si-Control, si-UBQLN1/2/4, treated with 50 μM AsNaO2 for 12 h post 48 h transfection, and stained with Hoechst. White arrows indicate larger α-syn-EGFP condensates." (*b*) Quantification of the number of α-syn-EGFP condensates (>3 μm^2) per cell. *$p < 0.05$, N.S., nonsignificant (Dunnett's test, versus si-Control/$AsNaO_2$). Nine images were quantified per condition. Values are the means ± SDs. (*E*) UBQLN2-KO, UBQLN1-KO, or si-UBQLN4-transfected α-syn(A53T)-EGFP/SH-SY5Y cells were treated with 50 μM $AsNaO_2$ for 12 h. Sarkosyl-soluble and -insoluble fractions were analyzed by SDS-PAGE and immunoblotting.

Figure 4. SO286 binds to the STI1 regions of UBQLN2.
(*A*) Structures of SO286 and biotin–SO286. (*B*) Surface plasmon resonance (SPR) analysis of biotin–SO286 reactivity with UBQLN2. The vertical axis represents the amount of binding in the resonance unit (RU). (*C*) (*a*) Illustration of the domain deletion mutants of UBQLN2. (*b*) SPR analysis of biotin–SO286 reactivity with the UBQLN2 deletion mutants. The vertical axis represents the amount of binding in the resonance unit (RU). (*D*) SPR analysis of biotin–SO286 reactivity with UBQLN2 (ΔSTI1-1) (*a*) and UBQLN2 (ΔSTI1-2) (*b*). The vertical axis represents the amount of binding in the RU. (*E*) Fluorescence microscopy images show solutions of the 10 μM UBQLN2 construct (1% DyLight488-labeling) after incubation at 37 °C for the indicated hours in the presence of SO286. (*F*) FRAP of UBQLN2 droplets in the presence of SO286. (*a*) Plots display average FRAP recovery curves from 10 separate droplets. Values are the means ± SDs. (*b*) Quantification of fractional recovery at 70 s after photobleaching from 10 separate droplets. ****$p < 0.0001$ (Dunnett's test, versus 72 h/Control). Values are the means ± SDs. (*G*) (a) Immunoprecipitated FLAG-UBQLN2 and HA-UBQLN2 were incubated with SO286. FLAG-UBQLN2 was pulled down with anti-FLAG beads, eluted with FLAG peptide, and immunoblotted. (*b*) Quantification of HA-

UBQLN2 intensity. **p < 0.01, N.S., nonsignificant (Dunnett's test, versus SO286 [0 μM]). Values are the means ± SDs.

Figure 5. SO286 inhibits α-syn aggregation within UBQLN2 droplets.
(*A*) (*a*) Immunoprecipitated α-syn-FLAG and recombinant HA-UBQLN2 were incubated with SO286. α-syn-FLAG was pulled down with anti-FLAG beads, eluted with the FLAG peptide, and immunoblotted. (*b*) Quantification of HA-UBQLN2 intensity. **p < 0.01, ***p < 0.001 (Dunnett's test, versus SO286 [0 μM]). Values are the means ± SDs. (*B*) Fluorescence microscopy images showing mixed solutions of 10 μM UBQLN2 construct (1% DyLight488-labeling) and 10 μM α-syn construct (1% DyLight633-labeling) in the presence of 20 μM SO286. (*C*) Each UBQLN (1 μM) was premixed with SO286 (0.25 mM) before being mixed with α-syn (1 μM), and the percentage area covered by proteins (α-syn and UBQLN1, UBQLN2, or UBQLN4) was measured. Values were calculated from HS-AFM images from three independent experiments. (*D*) Quantification of fractional recovery at 70 s after photobleaching from 10 separate droplets. ****p < 0.0001 (Dunnett's test, versus 96 h/Control). Values are the means ± SDs. (*E*) Fluorescence microscopy of UBQLN2/α-syn fibrils from droplets in LLPS buffer with 3% PEG and SO286 (10 μM each, 1% DyLight-labeled)(*F*) α-Syn(WT)-EGFP/SH-SY5Y cells were treated with 50 μM $AsNaO_2$ for the indicated hours in the presence of 20 μM SO286 and immunostained with anti-UBQLN2 and Hoechst. UBQLN2 droplets and large α-syn-EGFP condensates are indicated by white arrows. (*G*) α-Syn(WT)-EGFP/SH-SY5Y cells were treated with 50 μM $AsNaO_2$ for the indicated hours in the presence of 20 μM SO286 before being immunostained with anti-UBQLN2 and ThS. UBQLN2 droplets are indicated by white arrows. (*H*) α-Syn(WT)-EGFP/SH-SY5Y cells were treated with 50 μM $AsNaO_2$ for 12 h in the presence of 20 μM SO286. Cell lysates of the sarkosyl-soluble and -insoluble fractions were subjected to SDS-PAGE and immunoblotted with the indicated antibodies.

Supplementary Figure S1. α-Syn aggregates within UBQLN2 droplets *in vitro*.
(*A*) Fluorescence microscopy images of mixed solutions of 10 μM UBQLN2 or ΔUBL/UBQLN2 (1% DyLight488-labeling) and 10 μM α-syn construct (1% DyLight633-labeling) after incubation at 37 °C for the indicated periods. *(B*) Fluorescence microscopy images showing the disassembly of UBQLN droplets incorporating α-syn after the addition of 10% 1,6-HD.*(C)* Fluorescence microscopy images of partial droplet photobleaching for UBQLN2 (a), UBQLN1 (b), and UBQLN4 (c) droplets incorporating α-syn.

Supplementary Figure S2. α-Syn directly interacts with UBQLN2.
(*A* and *B*) (*a*) Illustrations of the UBQLN2 mutant with successive N-terminal deletions (*A*) or successive C-terminal deletions (*B*). (*b*) Each UBQLN2-HA mutant was subjected to SDS-PAGE and stained with Coomassie brilliant blue (CBB). (*c*) Each UBQLN2-HA mutant was

subjected to SDS-PAGE and transferred onto a membrane. The membrane was then incubated with recombinant His-α-syn, followed by detection using an anti-α-syn antibody.

Supplementary Figure S3. α-Syn aggregates within UBQLN2 droplets in cultured cells.
(*A*) Fluorescence microscopy of droplet photobleaching in α-Syn(WT)-EGFP/SH-SY5Y cells treated with 50 μM $AsNaO_2$ for the indicated hours. The bleached area is indicated by a dashed circle.*(B)* (*a*) Immunoblot of Control KO, UBQLN1 KO, and UBQLN2 KO α-syn(A53T)-EGFP/SH-SY5Y cell lysates. (*b*) Fluorescence microscopy of these cells after 12 h $AsNaO_2$ (50 μM) treatment, stained with Hoechst. White arrows indicate large α-syn-EGFP condensates. (*c*) Quantification of condensates (>3 μm²) per cell. **p < 0.01, ***p < 0.001, ****p < 0.0001, N.S. (two-way ANOVA, Tukey's test). Nine images per condition; mean ± SD.(*C*) (*a*) Fluorescence microscopy of α-syn(WT)-EGFP/SH-SY5Y cells with UBQLN knockdown. Cells transfected with si-Control, si-UBQLN1, si-UBQLN2, or si-UBQLN4 were treated with puromycin (10 μg/mL, 6 h) and stained with Hoechst. (*b*) Quantification of condensates (>3 μm²) per cell. **p < 0.01, ***p < 0.001, N.S. (Dunnett's test, vs. si-Control/puromycin). Ten images per condition; mean ± SD.

Supplementary Figure S4. SO286 binds to STI1 regions of UBQLN2.
(*A*) Surface plasmon resonance analysis of biotin–SO286 reactivity with UBQLN1 (*a*) and UBQLN4 (*b*). The vertical axis represents the amount of binding in the resonance unit (RU). (*B*) (*a*) Fluorescence microscopy images showing 10 μM solutions of each UBQLN construct (1% DyLight488-labeling) after incubation at 37 °C for 24 h in the presence of SO286. The number and size of the droplets of UBQLN 2 (*b*), UBQLN1 (*c*), and UBQLN4 (*d*) were quantified. N.S., nonsignificant (Dunnett's test, versus SO286 [0 μM]). Three images were quantified per condition. Values are the means ± SDs.
(*C*) Fluorescence microscopy images of partial droplet photobleaching experiments.

Supplementary Figure S5. SO286 inhibits α-syn aggregation within UBQLN2 droplets.
(*A*) Fluorescence microscopy images showing mixed solutions of 10 μM UBQLN2 construct (1% DyLight488-labeling) and 10 μM α-syn construct (1% DyLight633-labeling) in the presence of 2 μM and 7 μM SO286.(*B*) Effects of SO286 on the spinodal decomposition-like patterns of α-syn and UBQLN2 (*a,b*), UBQLN1 (*c,d*), or UBQLN4 (*e,f*). Each UBQLN (1 μM) was premixed with (*a,c,e*) or without (*b,d,f*) SO286 (0.25 mM) before being mixed with α-syn (1 μM). (*C*) FRAP analysis of UBQLN2 droplets with α-syn and SO286: (a) Fluorescence microscopy images of partial photobleaching for UBQLN2 and α-syn.
(*b*) Plots display average FRAP recovery curves from 10 separate droplets of UBQLN2 and α-syn. Values are the means ± SDs. (*D*) Quantification of the number of α-syn-EGFP puncta (>3 μm²) per cell from image of Fig. 5B. **p < 0.01, ***p < 0.001 (Dunnett's test, versus $AsNaO_2$). Five images were quantified per condition. Values are the means ± SDs.(*E*) α-

Syn(A53T)-EGFP/SH-SY5Y cells were treated with 50 μM $AsNaO_2$ for 12 h in the presence of 20 μM SO286.Sarkosyl-soluble and -insoluble fractions were subjected to SDS-PAGE and immunoblotted with the indicated antibodies.

5

Figure 1.

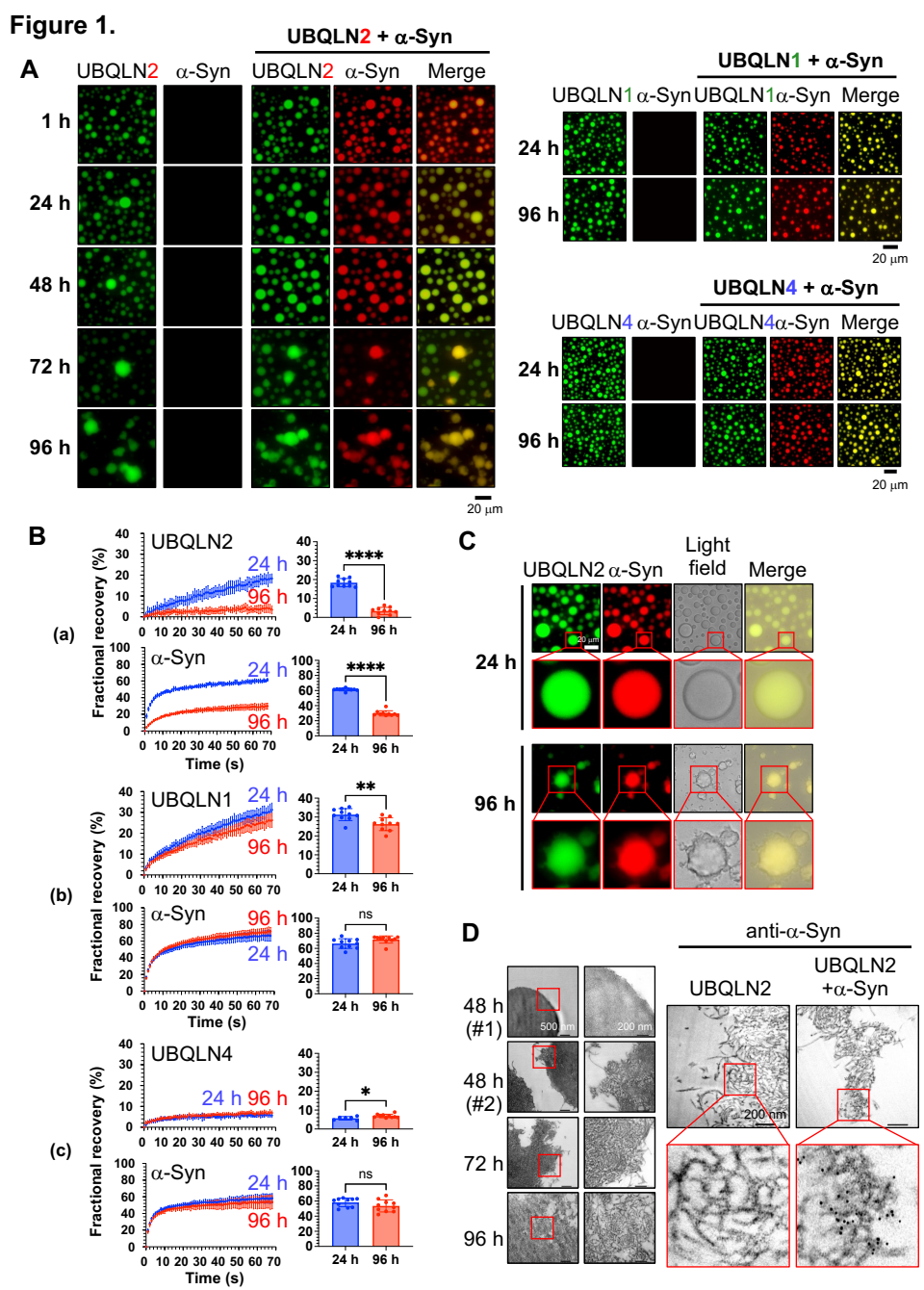
A
UBQLN2 + α-Syn
UBQLN2
α-Syn
UBQLN2
α-Syn
Merge
1 h
24 h
48 h
72 h
96 h
20 μm
UBQLN1 + α-Syn
UBQLN1
α-Syn
UBQLN1
α-Syn
Merge
24 h
96 h
20 μm
UBQLN4 + α-Syn
UBQLN4
α-Syn
UBQLN4
α-Syn
Merge
24 h
96 h
20 μm
B
(a)
UBQLN2
24 h
96 h
α-Syn
24 h
96 h
(b)
UBQLN1
24 h
96 h
α-Syn
96 h
24 h
(c)
UBQLN4
24 h 96 h
α-Syn
24 h
96 h
Fractional recovery (%)
Time (s)
0 10 20 30 40 50 60 70
24 h
96 h
****
****
**
ns
*
ns
C
UBQLN2
α-Syn
Light field
Merge
24 h
96 h
20 μm
D
anti-α-Syn
UBQLN2
UBQLN2 +α-Syn
48 h (#1)
48 h (#2)
72 h
96 h
500 nm
200 nm
200 nm

Figure 2.

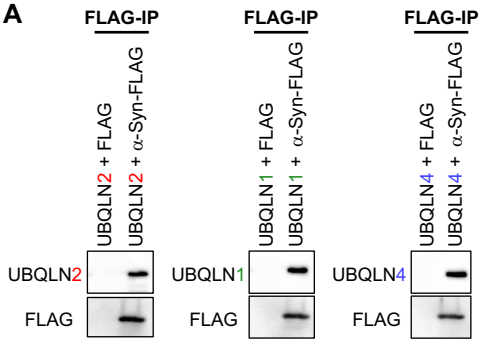
A
FLAG-IP
UBQLN2 + FLAG
UBQLN2 + α-Syn-FLAG
UBQLN2
FLAG
FLAG-IP
UBQLN1 + FLAG
UBQLN1 + α-Syn-FLAG
UBQLN1
FLAG
FLAG-IP
UBQLN4 + FLAG
UBQLN4 + α-Syn-FLAG
UBQLN4
FLAG

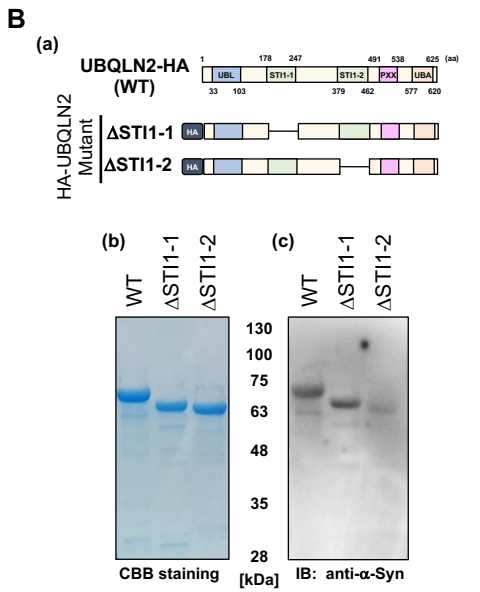
B
(a)
UBQLN2-HA (WT)
1
178
247
491
538
625
(aa)
UBL
STI1-1
STI1-2
PXX
UBA
33
103
379
462
577
620
HA-UBQLN2 Mutant
ΔSTI1-1
ΔSTI1-2
HA
(b)
WT
ΔSTI1-1
ΔSTI1-2
CBB staining
(c)
WT
ΔSTI1-1
ΔSTI1-2
IB: anti-α-Syn
130
100
75
63
48
35
28
[kDa]

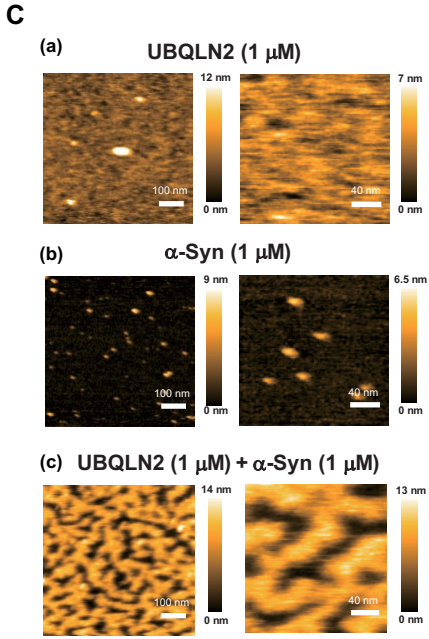
C
(a)
UBQLN2 (1 μM)
12 nm
0 nm
100 nm
7 nm
0 nm
40 nm
(b)
α-Syn (1 μM)
9 nm
0 nm
100 nm
6.5 nm
0 nm
40 nm
(c) UBQLN2 (1 μM) + α-Syn (1 μM)
14 nm
0 nm
100 nm
13 nm
0 nm
40 nm

Figure 3.

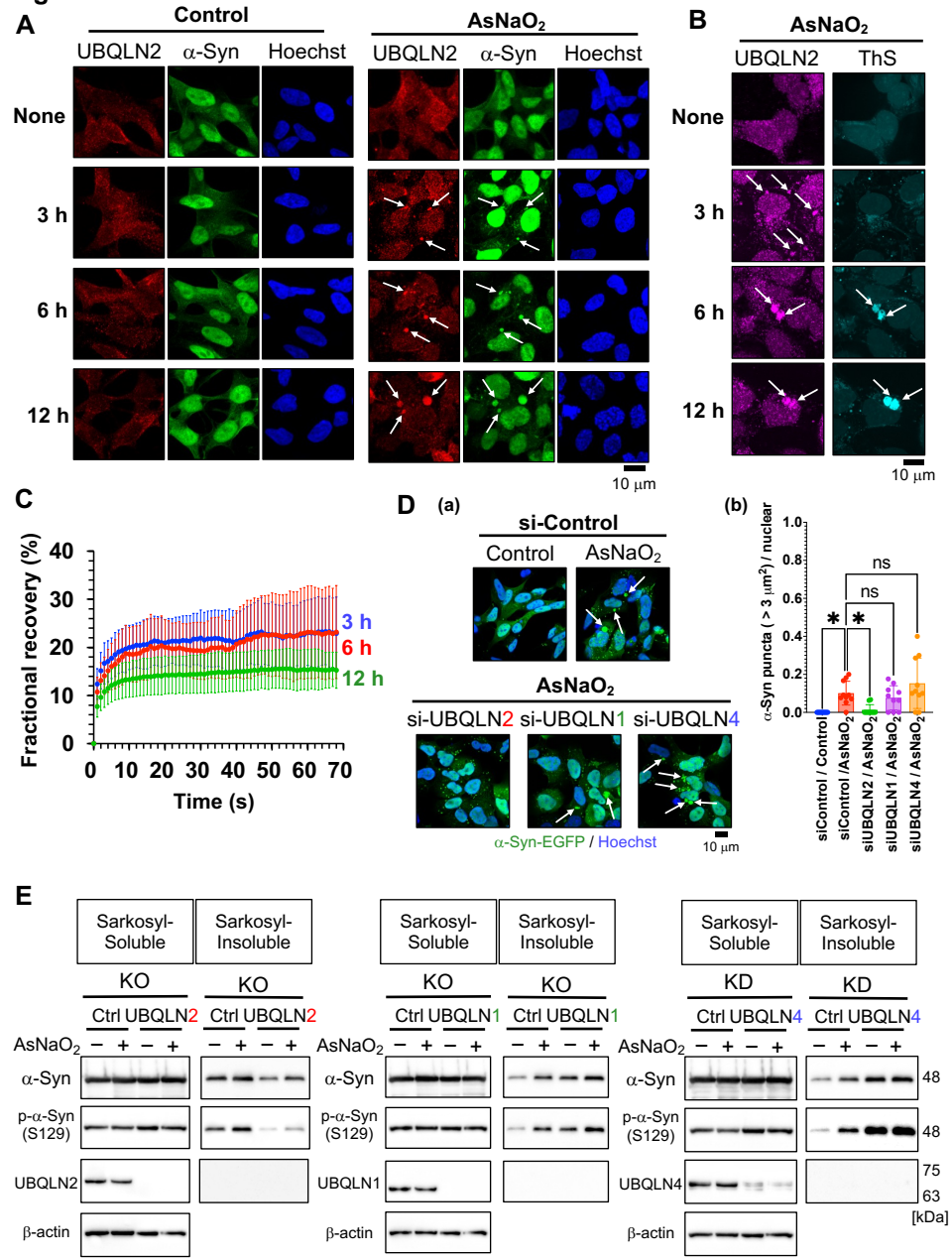
A
Control
AsNaO2
UBQLN2
α-Syn
Hoechst
None
3 h
6 h
12 h
10 μm
B
AsNaO2
UBQLN2
ThS
None
3 h
6 h
12 h
10 μm
C
Fractional recovery (%)
Time (s)
3 h
6 h
12 h
D
(a)
si-Control
Control
AsNaO2
AsNaO2
si-UBQLN2
si-UBQLN1
si-UBQLN4
α-Syn-EGFP / Hoechst
10 μm
(b)
α-Syn puncta (> 3 μm²) / nuclear
ns
ns
siControl / Control
siControl / AsNaO2
siUBQLN2 / AsNaO2
siUBQLN1 / AsNaO2
siUBQLN4 / AsNaO2
E
Sarkosyl-Soluble
Sarkosyl-Insoluble
KO
KD
Ctrl
UBQLN2
UBQLN1
UBQLN4
AsNaO2
α-Syn
p-α-Syn (S129)
β-actin
48
75
63
[kDa]

Figure 4.

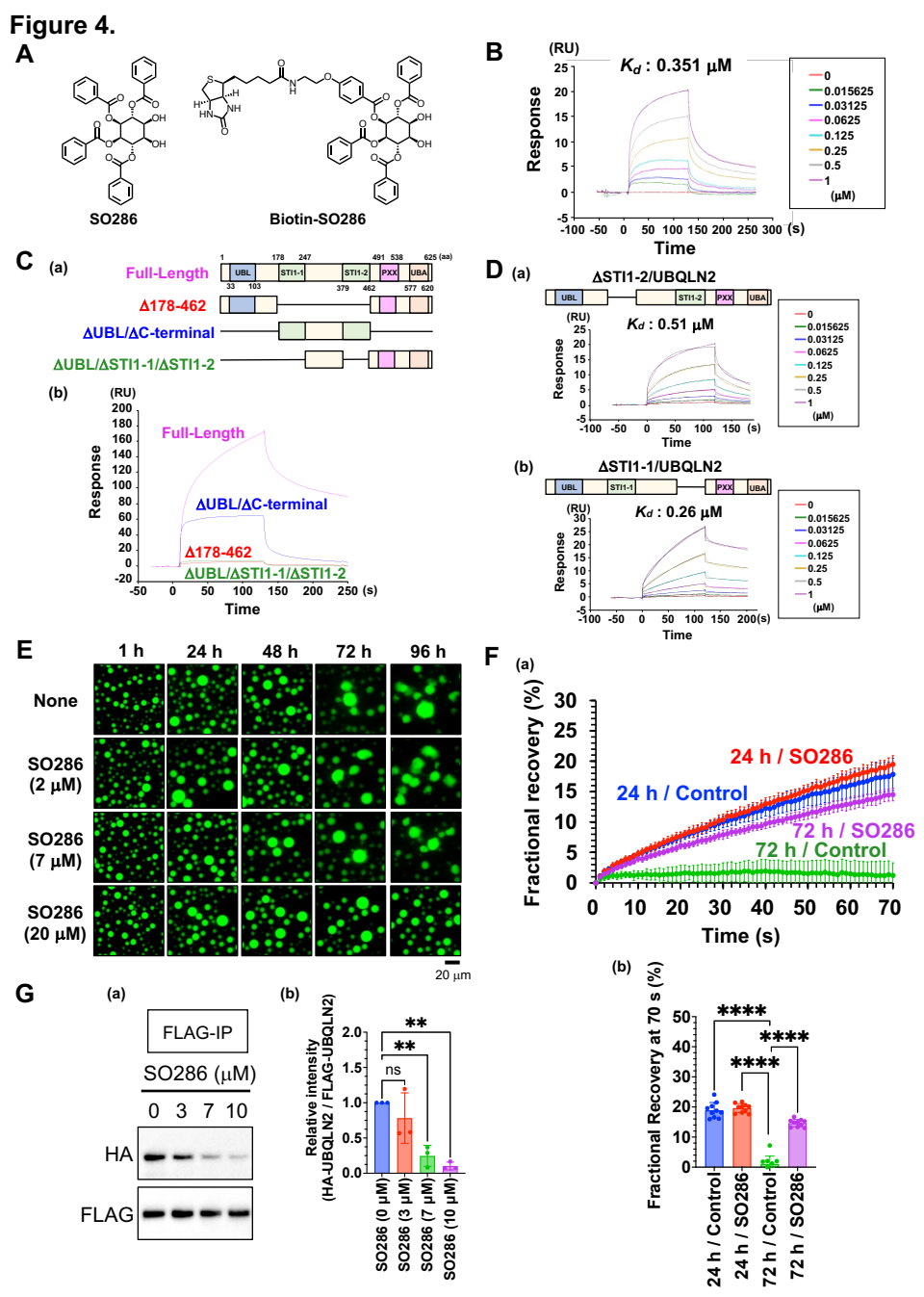
A
SO286
Biotin-SO286
B
(RU)
K_d : 0.351 μM
Response
Time
0
0.015625
0.03125
0.0625
0.125
0.25
0.5
1
(μM)
C
(a)
Full-Length
Δ178-462
ΔUBL/ΔC-terminal
ΔUBL/ΔSTI1-1/ΔSTI1-2
UBL
STI1-1
STI1-2
PXX
UBA
(b)
(RU)
Response
Time
Full-Length
ΔUBL/ΔC-terminal
Δ178-462
ΔUBL/ΔSTI1-1/ΔSTI1-2
D
(a)
ΔSTI1-2/UBQLN2
K_d : 0.51 μM
(b)
ΔSTI1-1/UBQLN2
K_d : 0.26 μM
E
1 h
24 h
48 h
72 h
96 h
None
SO286 (2 μM)
SO286 (7 μM)
SO286 (20 μM)
20 μm
F
(a)
Fractional recovery (%)
Time (s)
24 h / SO286
24 h / Control
72 h / SO286
72 h / Control
(b)
Fractional Recovery at 70 s (%)
****
24 h / Control
24 h / SO286
72 h / Control
72 h / SO286
G
(a)
FLAG-IP
SO286 (μM)
0 3 7 10
HA
FLAG
(b)
Relative intensity (HA-UBQLN2 / FLAG-UBQLN2)
ns
**
SO286 (0 μM)
SO286 (3 μM)
SO286 (7 μM)
SO286 (10 μM)

Figure 5.

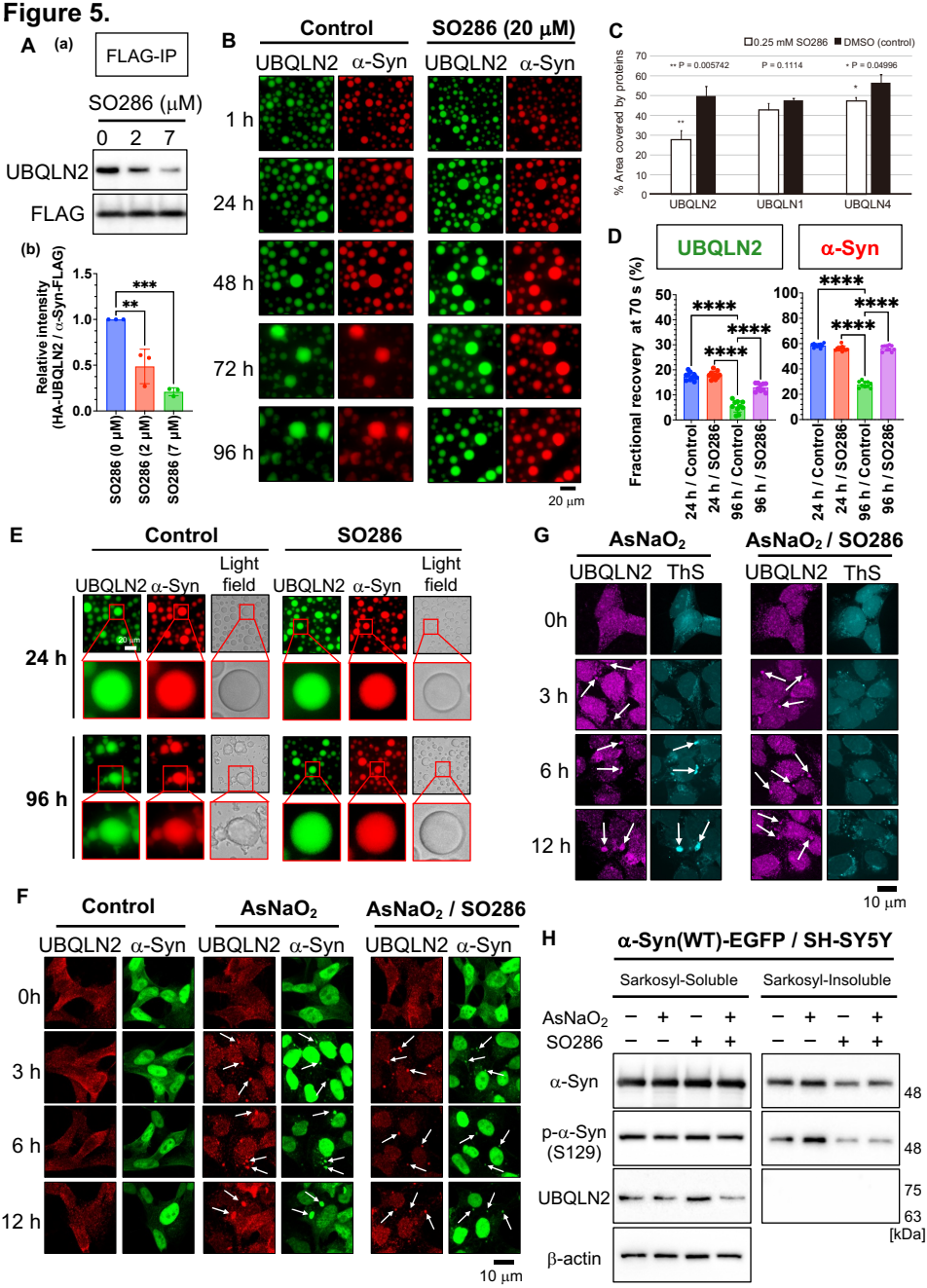
A
(a)
FLAG-IP
SO286 (μM)
0 2 7
UBQLN2
FLAG
(b)
Relative intensity (HA-UBQLN2 / α-Syn-FLAG)
1.5
1.0
0.5
0.0
**
***
SO286 (0 μM)
SO286 (2 μM)
SO286 (7 μM)
B
Control
SO286 (20 μM)
UBQLN2 α-Syn
UBQLN2 α-Syn
1 h
24 h
48 h
72 h
96 h
20 μm
C
0.25 mM SO286
DMSO (control)
% Area covered by proteins
70
60
50
40
30
20
10
0
** P = 0.005742
P = 0.1114
* P = 0.04996
UBQLN2
UBQLN1
UBQLN4
D
UBQLN2
α-Syn
Fractional recovery at 70 s (%)
50
40
30
20
10
0
100
80
60
40
20
0
****
24 h / Control
24 h / SO286
96 h / Control
96 h / SO286
E
Control
SO286
UBQLN2 α-Syn
Light field
UBQLN2 α-Syn
Light field
24 h
96 h
20 μm
G
AsNaO2
AsNaO2 / SO286
UBQLN2 ThS
UBQLN2 ThS
0h
3 h
6 h
12 h
10 μm
F
Control
AsNaO2
AsNaO2 / SO286
UBQLN2 α-Syn
UBQLN2 α-Syn
UBQLN2 α-Syn
0h
3 h
6 h
12 h
10 μm
H
α-Syn(WT)-EGFP / SH-SY5Y
Sarkosyl-Soluble
Sarkosyl-Insoluble
AsNaO2 − + − + − + − +
SO286 − − + + − − + +
α-Syn
p-α-Syn (S129)
UBQLN2
β-actin
48
48
75
63
[kDa]

Supplementary Figure S1.

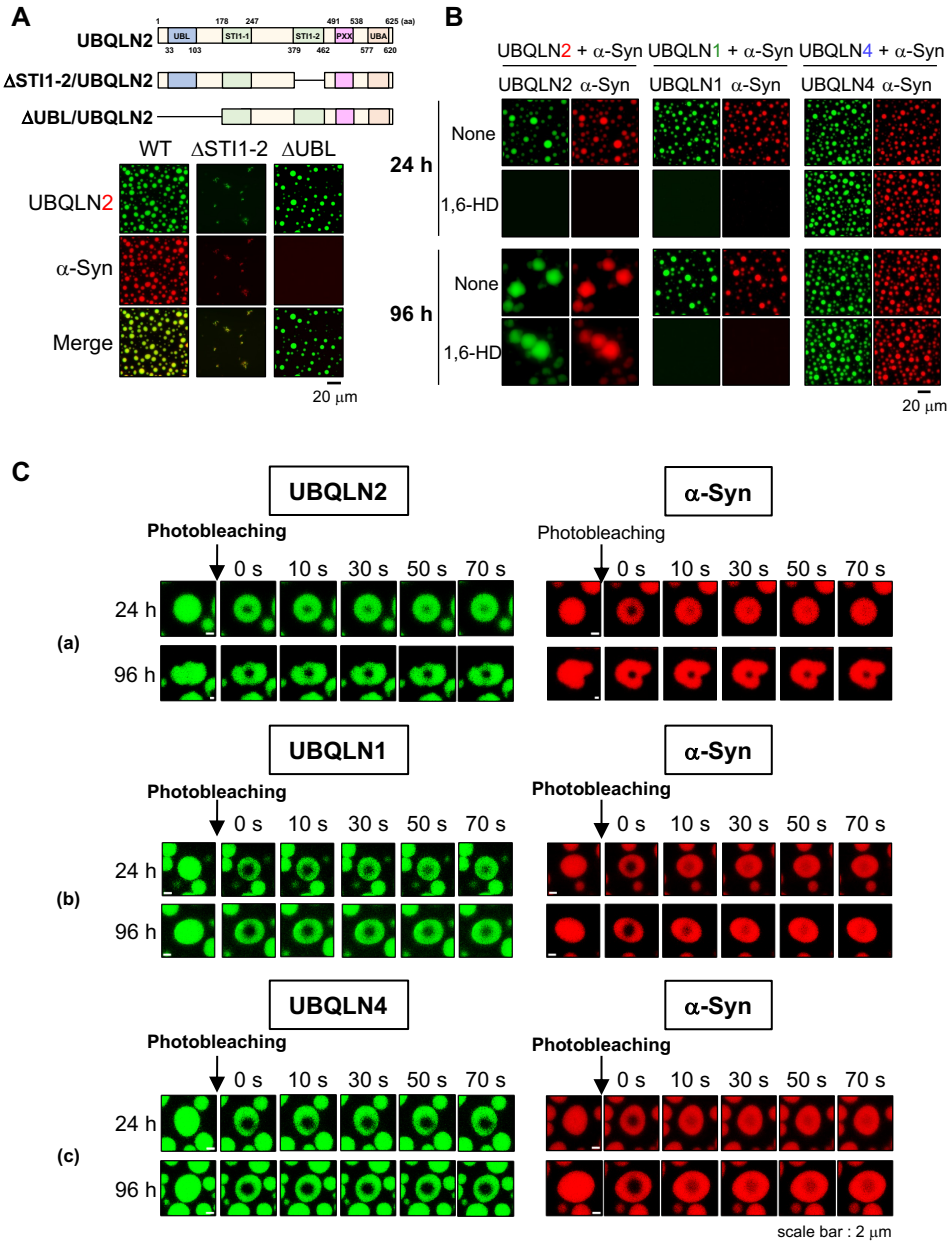

Supplementary Figure S2.

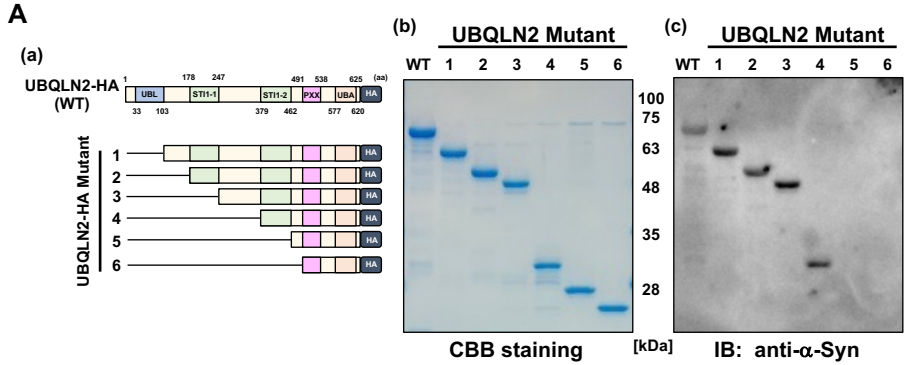

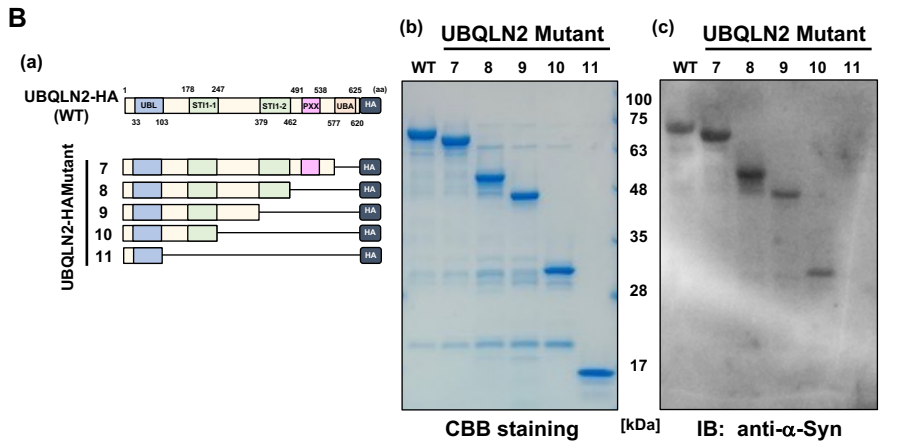

Supplementary Figure S3.

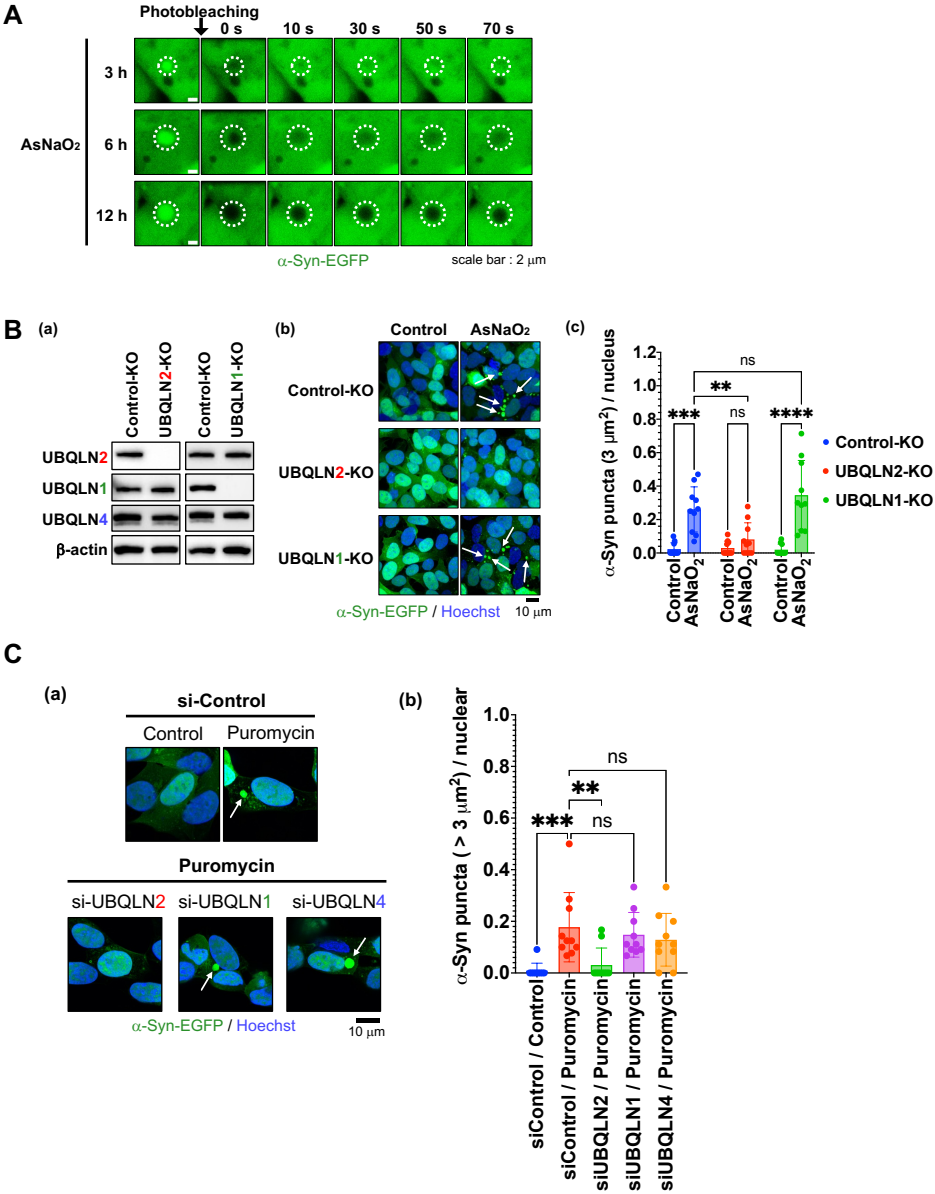

Supplementary Figure S4.

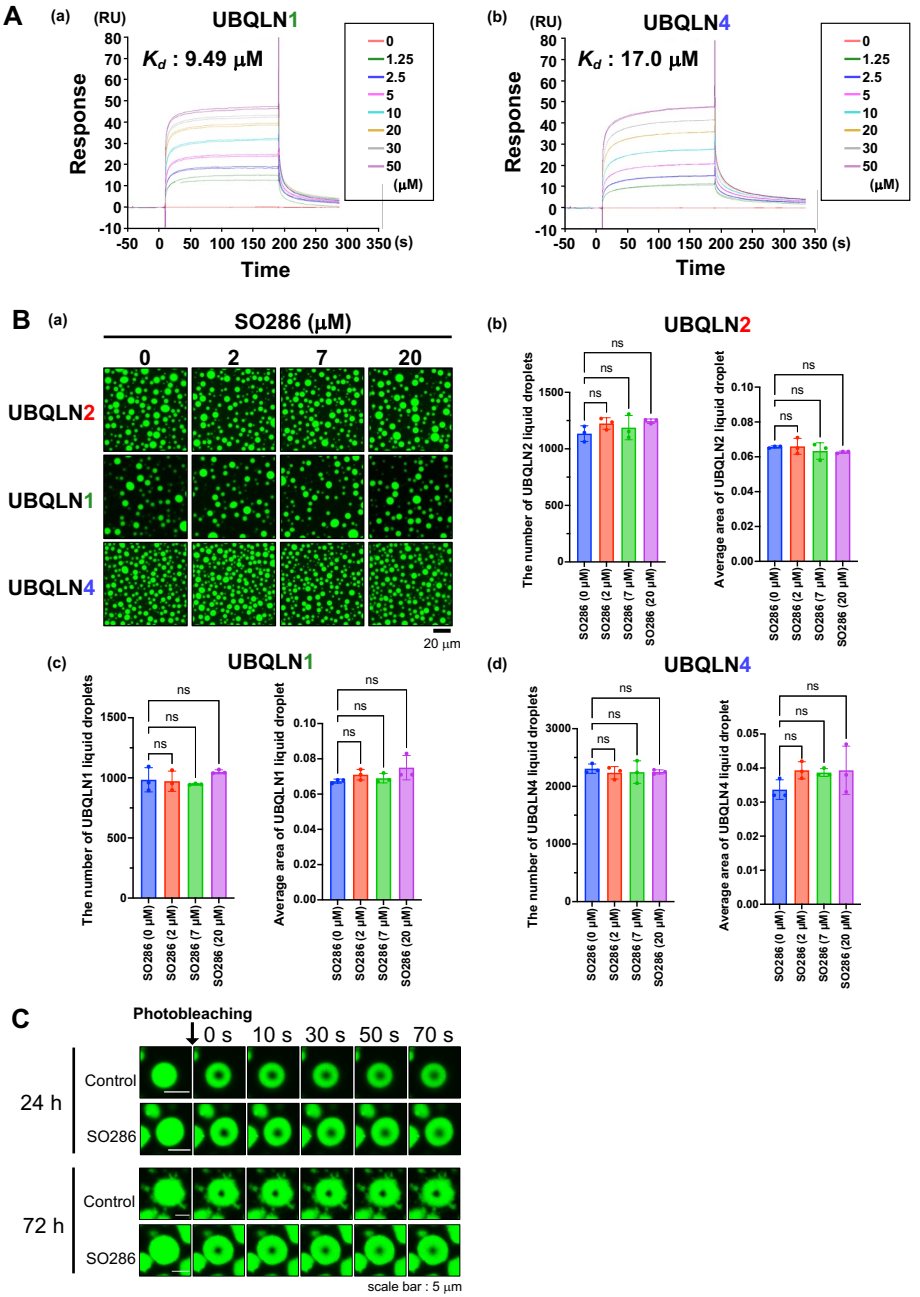
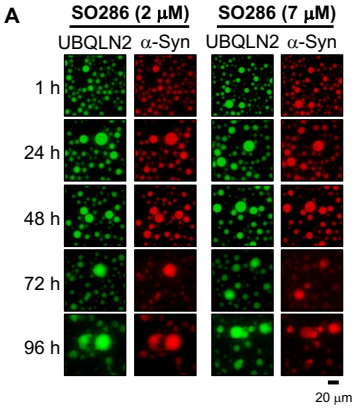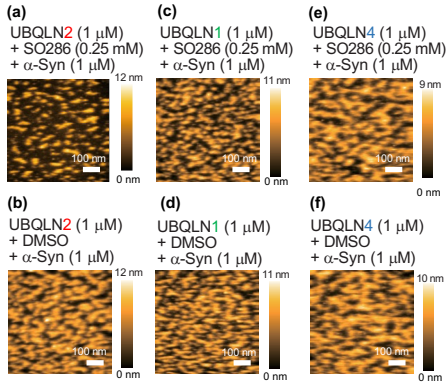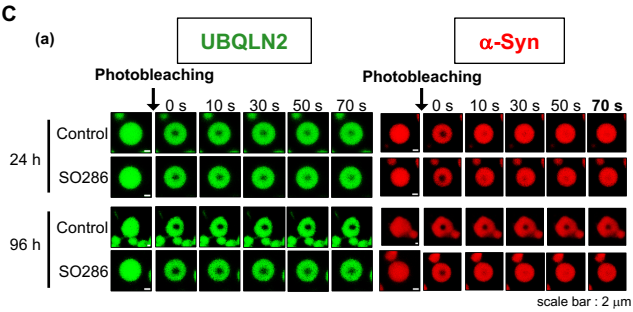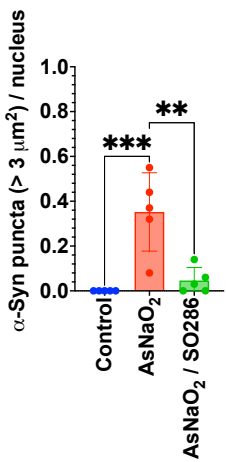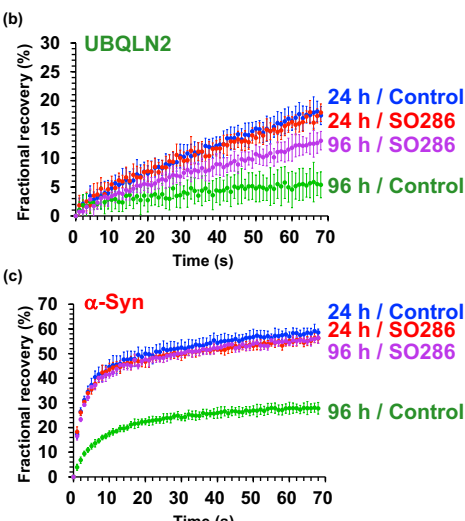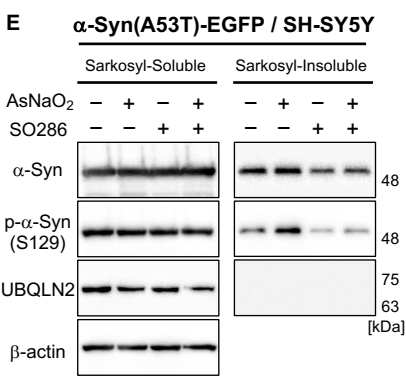
Supplementary Figure S5.